

## Reply to RC1

The manuscript “Significant contribution of organics to aerosol liquid water content in winter in Beijing, China” present a filed study in 2017 in Beijing China, focusing the aerosol liquid water content (ALWC). ALWC was derived from using the growth factor (GF) measured at 90% RH at three particle sizes in nucleation mode, Aiken and accumulation mode. ALWC was also calculated using ISORROPIA II model with the chemical composition characterized by AMS as input. It was found that generally  $ALWC_{HTDMA}$  correlates with  $ALWC_{ISORROPIA}$  at high RH, but not at  $RH < 60\%$ . Including  $ALWC_{org}$ , the ALWC contributed by organics, i.e.,  $ALWC_{ISORROPIA} + ALWC_{org}$  improved the correlation with ALWC (HTDMA), especially at lower RH. The contribution of organic to total ALWC was  $30 \pm 22\%$ . ALWC correlated with mass concentration of sulfate, nitrate and SOA. Accumulation mode was found to contribute the largest portion to ALWC. In case study, ALWC contributed by organics may play an important role in the initial stage of haze event. The manuscript addresses ALWC, which an important parameter in atmospheric chemistry. The manuscript fits the scope of ACP. I have several comments which need to be addressed before the manuscript is considered to be published in ACP.

### General comments

1. The manuscript emphasized the role of organics in total ALWC. The value fraction  $30 \pm 22\%$  has a large uncertainty, suggesting a large variation of the contribution and likely a much smaller contribution of organics total in some cases. Also, the conclusion is in contrast with Z. Wu et al., 2018, showing dominant role of inorganics in ALWC, as the authors also cited. The variations and the difference from the literature needs to be discussed in the manuscript.

**Re: Good suggestion. This is likely related with the variation in mass fraction and hygroscopicity parameter of organics ( $\kappa_{org}$ ). To demonstrate this, we calculated the variation of the fraction of  $ALWC_{Org}$  in total ALWC ( $ALWC_{HTDMA}$ ) with the ambient relative humidity (RH) and presented in Fig. R1. It is seen that the contribution of organics to total ALWC varies strongly. The mass concentration of inorganics increases more than that of organics as RH increases, leading to a lower mass fraction of organics in the case of high ambient RH. Figure R1 also shows the  $ALWC_{Org}$  fraction increases significantly with the increase of  $\kappa_{org}$ . All these help explain a large variation in the  $ALWC_{Org}$  contribution to total ALWC. Considering the distinct differences in ambient RH and  $\kappa_{org}$  between clean and polluted periods, we calculated respectively the fraction of  $ALWC_{Org}$  during the two periods. There is a higher  $ALWC_{Org}$  fraction ( $33\% \pm 23\%$ ) during clean periods than that during polluted periods ( $26\% \pm 11\%$ ). Yet, there is little variability of  $ALWC_{Org}$  fraction during polluted periods. The larger variability in  $ALWC_{Org}$  fraction during clean periods is likely caused by the highly variable  $\kappa_{org}$  when the ambient RH is low. In summary, the mass fraction of organics and  $\kappa_{org}$  are important contributors to total ALWC, which was not investigated in Z. Wu et al. (2018). Our results also suggest inorganics (nitrate and sulfate) play key roles in determining ALWC, which is similar to Z. Wu et al. (2018).**

We have added the Figure R1 in the manuscript (Figure 4) and the discussion above in line 311-323.

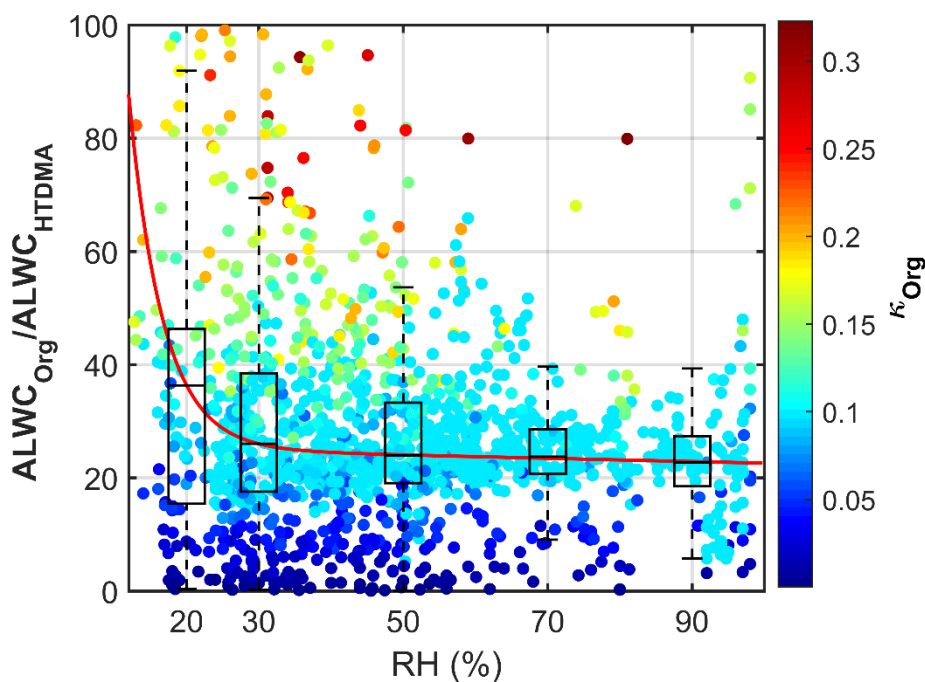


Figure R1. The variation of the fraction of  $ALWC_{Org}$  in total  $ALWC$  ( $ALWC_{HTDMA}$ ) with the ambient relative humidity (RH). The color of the dots denotes the hygroscopicity parameter of organics ( $\kappa_{Org}$ ). The boxes show the fraction of  $ALWC_{Org}$  with the 25th, 50th, and 75th percentiles. The extremities show the 5th and 95th percentiles. The red line shows the fitting curve with the function:  $y = ae^{bx}$ .

2. Some important details are lacking (see specific comments).

### Specific

### comments

1. Line 77 "...its factors..." is confusing. Please specify.

Re: Good suggestion. The corresponding sentence was revised as "Overall, investigating the formation of SA and haze in North China requires an examination of ALWC and its factors including aerosol particle number size distribution (PNSD), aerosol chemical composition and ambient related humidity (RH) in this region" in line 77-78.

2. Line 156-159, at which three sizes the GF were measured?

Re: During this campaign, the H-TDMA was used to measure the GF at five particle sizes (40, 80, 110, 150, 200nm), which has been described in section 2.2. Then we follow the method of Chen et al. (2012) to calculate size-resolved GFs under different RHs, which is presented in section 3.1.

3. Line 162, the assumption of constant  $\kappa$  in each mode may result in uncertainty in ALWC. It may be worthy discussing these lines 237-253.

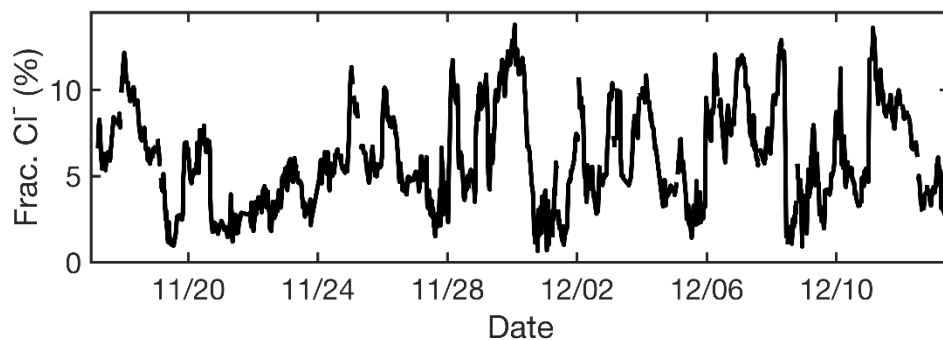
Re: We assumed a constant  $\kappa$  in each mode based on the assumption that aerosols in a specific mode have common sources and experience similar aging processes, so  $\kappa$  in one mode should be the same due to the same chemical compositions (Chen et al., 2012). This may lead to a small uncertainty in size-resolved GFs at different RHs, resulting in a deviation in ALWC calculation. The following is added: "the assumption of constant  $\kappa$  in each mode may lead to a small uncertainty in size-resolved GFs at different RHs, resulting in small deviations in ALWC calculation. This may be another reason for the difference between  $ALWC_{HTDMA}$  and  $ALWC_{ISO}$ ." in the line 243-245.

4. Lines 237-253, for the chemical composition measured by AMS, do the authors use bulk composition or size resolved composition? This can also contribute to the ALWC derived by ISORROPIA.

74 Re: The bulk chemical composition measured by HR-AMS was used to simulate ALWC from  
75 ISOPPOPIA II model. Therefore, the simulated ALWC from ISOPPOPIA II denotes the total ALWC,  
76 which can't consider the contribution of organics on ALWC. The size resolved aerosol chemical  
77 composition data are hard to use in this model. We have added the sentence as "The bulk chemical  
78 composition was used in model." in line 188.

79  
80 5. Lines 204-227, in deriving ALW<sub>Corg</sub>, among inorganics, only sulfuric acid, ammonium sulfate,  
81 ammonium hydrogen sulfate, and ammonium nitrate were considered. Actually, chloride is also  
82 present, as this study found. The can result in uncertainty in ALW<sub>Corg</sub>.

83 Re: The chloride detected by AMS may be from organics, and it is hard to be verified. So most previous  
84 papers didn't consider chloride when studying aerosol hygroscopicity (e.g., Gysel et al., 2007; Sjogren  
85 et al., 2008; Guo et al., 2015; Cerully et al., 2015). In addition, the mass concentration of chloride is  
86 always low in PM<sub>1</sub>. Figure R2 show the time series of chloride mass concentration during the sample  
87 period. It shows the average mass fraction of chloride is only 6% ± 3%. We added the sentence as in  
88 line 223-224 as "The chloride was not taken into account in ion-pairing because its source is hard to  
89 determine. This may result in a minor uncertainty in  $\kappa$  calculation."



90  
91 **Figure R2. Time series of the mass fraction of chloride.**

92  
93 6. Line 281, how is b derived?

94 Re: b is derived by curve fitting through the data of ALW<sub>C<sub>HTDMA</sub></sub> and RH using the fitting function  $y =$   
95  $ae^{bx}$ . This is clarified as "b is derived according to the relationship between ALW<sub>C<sub>HTDMA</sub></sub> and RH that  
96 is fitted by the function  $y = ae^{bx}$ ." in line 287-288.

97  
98 7. Line 283, how are POA and SOA derived? Did the authors use PMF?

99 Re: The POA and SOA are derived using PMF. The sentence was added as "The positive matrix  
100 factorization (Paatero and Tapper, 1994) was applied on the organic aerosols (OA) spectral matrices  
101 to identify POA and SOA." in line 290-291.

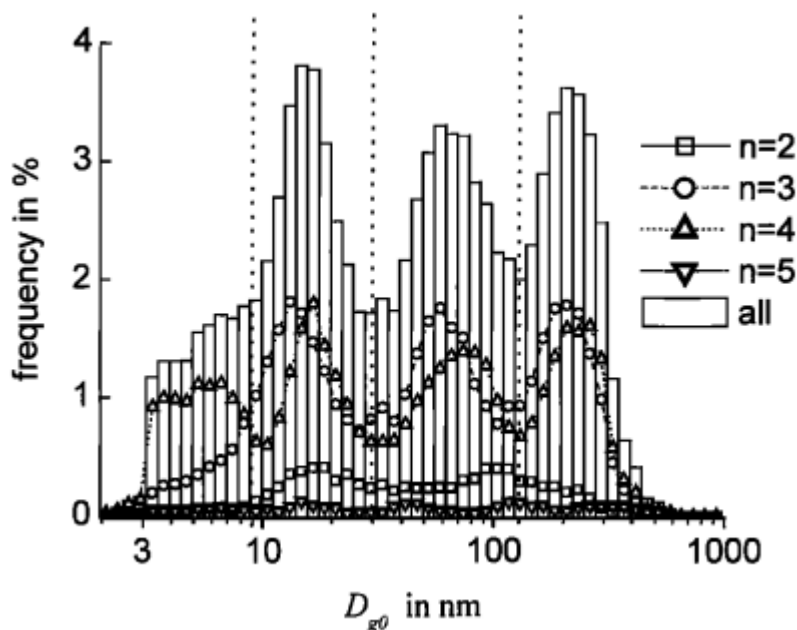
102  
103 8. Section 4.2.2, Fig. 4 does not provide new information to the discussion. The accumulation mode  
104 contributed dominant hygroscopic materials and ALWC to total ALWC. Naturally, the correlations are  
105 better.

106 Re: The analysis of the relationship between ALWC and the different modes under five different RH  
107 condition is for further evaluation of the impact of PNSD on the ALWC. Figure 4 shows the average  
108 contribution of different mode particles to ALW<sub>C<sub>HTDMA</sub></sub> ( $f_{ALWC}$ ) and the slope of the best linear  
109 regression. Figure 4 also shows that ALWC increases slightly as the volume concentration of  
110 accumulation mode particles increases under RH < 70 % conditions (slope < 0.001), but increases are  
111 stronger under higher RH conditions, especially under RH > 90 % conditions (slope = 0.0041). This  
112 suggests that there are more accumulation mode SA formed due to multiphase chemical reactions  
113 under high ambient RH conditions. Besides, Figure 4 also shows that the correlation between the  
114 Aitken mode particles and ALWC is enhanced significantly under RH > 90 % conditions, which

115 suggests that the Aitken mode can also absorb a significant amount of water when RH is higher than  
116 90%. So, we think Fig. 4 is necessary to discuss the completeness of ALWC.

117  
118 9. Line 323-325, such a statement is not necessarily true because many “processed” mineral particles  
119 are highly hygroscopic, such as  $\text{Ca}(\text{NO}_3)_2$ , or  $\text{MgSO}_4$ , as shown by many field and laboratory studies.  
120 Re: Agree, this statement is not accurate. Some mineral particles are hygroscopic and can impact  
121 ALWC. However, these particles are mainly in the coarse mode (Hussein et al., 2004; S. Liu et al.,  
122 2008). Bian et al. (2014) and Tan et al. (2017) found the ALWC contributed by coarse mode particles  
123 exists but not substantial. Because there were no APS data in this campaign, the coarse-mode particles  
124 with diameters greater than  $1\ \mu\text{m}$  are not considered in this study. The statement is revised as “Particles  
125 with diameters greater than  $1\ \mu\text{m}$  are not considered because some particles in the coarse mode are  
126 water soluble but their contribution on the ALWC is low (e.g., Hussein et al., 2004; S. Liu et al., 2008;  
127 Bian et al., 2014; Tan et al., 2017).” In line 342-345.

128  
129 10. Line 321, why upper limit of Aitken mode is set at 110 nm?  
130 Re: In general, aerosol particles are separated into four modes in the diameter lower than  $1\ \mu\text{m}$   
131 according to their different origins (Whitby, 1978). And there are some different standards to separate  
132 them. Birmili et al. (2001) defined the particle modes based on a long-term observation data (Figure  
133 R3): “fresh” nucleation mode: 3-9 nm; “aged” nucleation mode: 9-30 nm; Aitken mode: 30-110 nm;  
134 accumulation mode (110-1000 nm). Bian et al. (2014) also set the diameter of Aitken mode between  
135 30nm and 110nm when parameterizing the particle size distribution using a multiple lognormal fitting  
136 function. Therefore, it’s thus reasonable to set the upper limit of Aitken mode at 110nm.



137  
138 **Figure R3. Frequency distribution of modal geometric mean diameters. Subsets of mode numbers 2-5 are included.**  
139 **The figure is from Birmili et al., (2001).**

140  
141 11. Line 320 (and 370), I am not sure whether using PNSD is proper here. The ALWC depends on the  
142 amount of hygroscopic materials, no matter which sizes they are present.

143 Re: The PNSD provides the information of the number concentration of particles at different sizes.  
144 ALWC not only depends on the number concentration of hygroscopicity particles but also depends on  
145 the particle size. Such as Aitken mode particles with small volume, because of the Kelvin effect,  
146 although the Aitken mode particles show a high hygroscopicity, they do not make a large contribution  
147 to ALWC. So, when Aitken mode particles and accumulation mode particles have the same

148 hygroscopicity and number concentration, the particles in the accumulation mode can contribute more  
149 to ALWC than that in Aitken mode because accumulation mode particles have larger volume.  
150 Furthermore, the particles in different sizes have different hygroscopicity because of their origins,  
151 which also affects the ALWC. So PNSD needs to be considered when studying ALWC. Bian et al.  
152 (2014) and Tan et al. (2017) also found that PNSD is an important factor of ALWC.

153  
154  
155  
156

#### 157 **Reference:**

- 158 Bian, Y. X., Zhao, C.S., Ma, N., Chen, J., Xu, W.Y.: A study of aerosol liquid water content based on hygroscopicity  
159 measurements at high relative humidity in the North China Plain, *Atmos. Chem. Phys.*, 14 (12), 6417–6426,  
160 <https://doi.org/10.5194/acp-14-6417-2014>, 2014.
- 161 Birmili, W., Wiedensohler, A., Heintzenberg, J., and Lehmann, K.: Atmospheric particle number size distribution in central  
162 Europe: Statistical relations to air masses and meteorology, *J. Geophys. Res.-Atmos.*, 106, 32005–32018,  
163 <https://doi.org/10.1029/2000JD000220>, 2001.
- 164 Cerully, K. M., Bougiatioti, A., Hite Jr., J. R., Guo, H., Xu, L., Ng, N. L., Weber, R., and Nenes, A.: On the link between  
165 hygroscopicity, volatility, and oxidation state of ambient and water-soluble aerosols in the southeastern United States,  
166 *Atmos. Chem. Phys.*, 15, 8679-8694, <https://doi.org/10.5194/acp-15-8679-2015>, 2015.
- 167 Chen, J., Zhao, C. S., Ma, N., Liu, P. F., Göbel, T., Hallbauer, E., Deng, Z. Z., Ran, L., Xu, W. Y., Liang, Z., Liu, H. J.,  
168 Yan, P., Zhou, X. J., and Wiedensohler, A.: A parameterization of low visibilities for hazy days in the North China  
169 Plain, *Atmos. Chem. Phys.*, 12, 4935–4950, <https://doi.org/10.5194/acp-12-4935-2012>, 2012.
- 170 Guo, H., Xu, L., Bougiatioti, A., Cerully, K. M., Capps, S. L., Hite Jr., J. R., Carlton, A. G., Lee, S.-H., Bergin, M. H., Ng,  
171 N. L., Nenes, A., and Weber, R. J.: Fine-particle water and pH in the southeastern United States, *Atmos. Chem. Phys.*,  
172 15, 5211-5228, <https://doi.org/10.5194/acp-15-5211-2015>, 2015.
- 173 Gysel, M., Grosier, J., Topping, D.O., Whitehead, J.D., Bower, J.N., Cubison, M.J., Williams, P.I., Flynn, M.J., McFiggans,  
174 G.B., Coe, H.: Closure study between chemical composition and hygroscopic growth of aerosol particles during  
175 TORCH2, *Atmos. Chem. Phys.*, 7 (24), 6131–6144, <https://doi.org/10.5194/acp-7-6131-2007>, 2007.
- 176 Hussein, T., Puustinen, A., Aalto, P. P., Mäkelä, J. M., Hämeri, K., and Kulmala, M.: Urban aerosol number size  
177 distributions, *Atmos. Chem. Phys.*, 4, 391–411, <https://doi.org/10.5194/acp-4-391-2004>, 2004.
- 178 Liu, S., Hu, M., Wu, Z., Wehner, B., Wiedensohler, A., and Cheng, Y.: Aerosol number size distribution and new particle  
179 formation at a rural/coastal site in Pearl River Delta (PRD) of China, *Atmos. Environ.*, 42, 6275–6283,  
180 <https://doi.org/10.1016/j.atmosenv.2008.01.063>, 2008.
- 181 Paatero, P., & Tapper, U. (2010). Positive matrix factorization: a non-negative factor model with optimal utilization of  
182 error estimates of data values. *Environmetrics*, 5(2), 111-126.
- 183 Sjogren, S., Gysel, M., Weingartner, E., Alfarra, M. R., Duplissy, J., Cozic, J., Crosier, J., Coe, H., and Baltensperger, U.:  
184 Hygroscopicity of the submicrometer aerosol at the high-alpine site Jungfraujoch, 3580 m a.s.l., Switzerland, *Atmos.*  
185 *Chem. Phys.*, 8, 5715-5729, <https://doi.org/10.5194/acp-8-5715-2008>, 2008.
- 186 Tan, H., Cai, M., Fan, Q., Liu, L., Li, F., & Chan, P. W., et al.: An analysis of aerosol liquid water content and related  
187 impact factors in pearl river delta, *Science of The Total Environment*, 579, 1822-1830,  
188 <https://doi.org/10.1016/j.scitotenv.2016.11.167>, 2017.
- 189 Whitby, K. T.: The physical characteristics of sulfur aerosols, *Atmos. Environ.*, 12, 135–159,  
190 <https://doi.org/10.1016/j.atmosenv.2007.10.057>, 1978.
- 191 Wu, Z., Wang, Y., Tan, T., Zhu, Y., Li, M., & Shang, D., et al.: Aerosol liquid water driven by anthropogenic inorganic  
192 salts: implying its key role in the haze formation over north china plain, *Environ. Sci. Technol. Lett.*, 5(3), 160-166,  
193 <https://doi.org/10.1021/acs.estlett.8b00021>, 2018.

194  
195

196

197

198



## Reply to RC2

199

200

201

202 This study uses two methods (by measuring aerosol hygroscopic growth factor and particle number  
203 size distribution and by thermodynamic equilibrium modeling in combination of measured aerosol  
204 chemical species) to estimate the aerosol liquid water content ALWC from a field campaign in winter  
205 Beijing and argues that organics contribute significantly to the total ALWC and further that organics-  
206 ALWC plays a role in the formation of secondary aerosols through multiphase reactions at the initial  
207 haze stage.

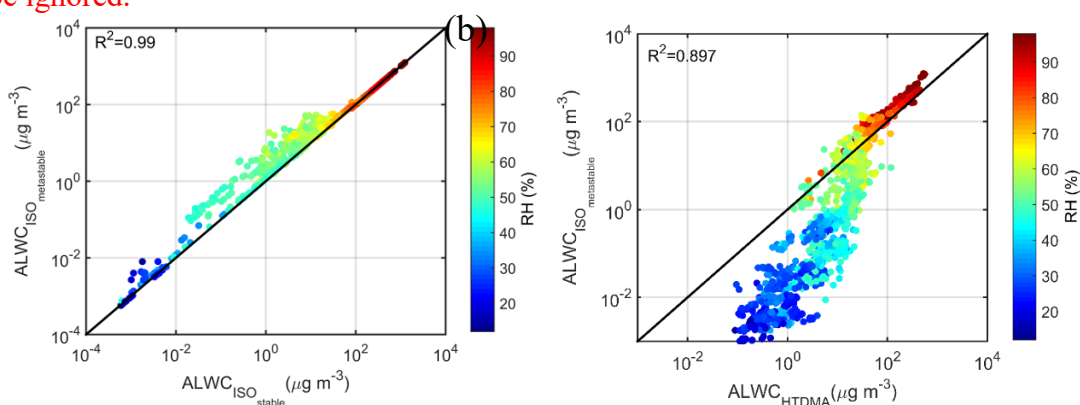
208

### 209 Major comments

210 There could be inconsistency in phase states between the two methods of ALWC. Here,  
211 thermodynamic modeling assumes that the aerosol particles are in a stable thermodynamic state. But  
212 the measurements of hygroscopic growth factor increase the RH to 90% that effectively leads to a  
213 metastable thermodynamic state for the sampled aerosol particles. My question is: if the authors repeat  
214 ALWC calculations of thermodynamic models assuming a metastable state, whether the results would  
215 change? For example, whether the underestimates in ALWC by ISORROPIA would disappear? I feel  
216 that this point should be clarified in this study since it is one of the major arguments of this manuscript  
217 and since this point also affects the other argument made in this study: whether organics ALWC plays  
218 a role in the formation of secondary aerosols through multiphase reactions at the initial haze stage.

219 **Re: Good suggestion. Bian et al. (2014) and Tan et al. (2017) both found the underestimation of ALWC**  
220 **simulated by ISOPPOPIA II model. Tan et al. (2017) used the ISOPPOPIA II model assuming the**  
221 **chemical species in the metastable state to simulate the ALWC, which also showed that the  $ALWC_{ISO}$**   
222 **was lower than  $ALWC_{HTDMA}$  for RH below 70%. Their explanation is the lack of hygroscopicity of**  
223 **organic particles which was not taken into account in ISOPPOPIA II model. Here we repeat ALWC**  
224 **simulation using ISOPPOPIA II model assuming the chemical species in metastable state. As shown**  
225 **in Fig. R1a, the simulated ALWC in metastable state ( $ALWC_{ISO\text{metastable}}$ ) is similar with that in stable state**  
226 **( $R^2 = 0.99$ ), which is similar with the results in Song et al. (2018). They also showed that the simulated**  
227 **ALWC in metastable state is similar with that in stable state at low RH in Beijing. Figure R1b further**  
228 **compares the simulated ALWC in metastable state and calculated ALWC, showing  $ALWC_{ISO\text{metastable}}$  is still**  
229 **lower than  $ALWC_{HTDMA}$ . Moreover, regardless of the result of ISOPPOPIA II model, the average**  
230 **organic ALWC we inferred accounts for 30%. And for low RH and high organics hygroscopicity, the**  
231 **average organic ALWC accounts for up to 58%, suggesting the contribution of organics to ALWC**  
232 **cannot be ignored.**

233 (a)



234

235 **Figure R1. The correlation analysis between (a)  $ALWC_{ISO\text{stable}}$  and  $ALWC_{ISO\text{metastable}}$  and (b)  $ALWC_{HTDMA}$  and  $ALWC_{ISO\text{metastable}}$ .**  
236  **$ALWC_{HTDMA}$  refers to calculated ALWC based on the measured growth factor and PNSDs,  $ALWC_{ISO\text{stable}}$  refers**  
237 **to simulated ALWC from the ISORROPIA II model assuming chemical species in the stable state.  $ALWC_{ISO\text{metastable}}$**   
238 **refers to simulated ALWC from the ISORROPIA II model assuming chemical species in the metastable state. The**  
239 **coefficient of determination  $R^2$  is given in each panel. The color of the dots denotes the ambient RH; the black solid**  
239 **line denotes the 1:1 line.**

240  
241  
242  
243  
244  
245  
246  
247  
248  
249  
250  
251  
252  
253  
254  
255  
256  
257  
258  
259  
260  
261  
262  
263  
264  
265  
266  
267  
268  
269  
270  
271  
272

**Minor and grammatical comments:**

Line 78: can the authors elaborate on what is the direct method to measured ALWC?

Re: To our knowledge, there are no techniques for measuring the ALWC directly (Kuang et al., 2018). The sentence has been revised as: “directly measuring real-time ALWC is not feasible yet because of technical limitations (Kuang et al., 2018).” in line 79.

Line 79: why the direct measurements of ALWC is especially difficult under high RH conditions? It seems to me that such measurements under low RH conditions are more difficult.

Re: Direct measurement of ALWC is not feasible at present, for any ambient RH conditions. A possible reason is that ALWC is sensitive to RH, but the RH of aerosol sample always changes inside any instrument.

Line 94: is should be was.

Re: Thanks, we have corrected it in the manuscript.

Line 160: show should be showed.

Re: Thanks, we have corrected it in the manuscript.

Line 215: I would be surprised if  $n_{\text{H}_2\text{SO}_4}$  were larger than 0. Would it be? Eq. 8: where is  $n_{\text{NH}_4\text{Cl}}$ ?

Re: No, the calculated  $n_{\text{H}_2\text{SO}_4}$  always equals to 0 in our campaign although the ion-pairing scheme (Gysel et al., 2007) used in this paper considers the contribution of  $\text{H}_2\text{SO}_4$  to inorganics.

Figure R2 show the time series of the mass fraction of chloride during the campaign. The chloride detected by AMS may be from organics, and it is hard to be verified. So most previous papers didn't consider the contribution of chloride when studying aerosol hygroscopicity (e.g., Gysel et al., 2007; Sjogren et al., 2008; Guo et al., 2015; Cerully et al., 2015). In addition, the mass concentration of chloride is always low in  $\text{PM}_{10}$ . As shown in Figure R2, the average mass fraction of chloride is only  $6\% \pm 3\%$ . We added the sentence as in line 223-224 as “In this paper, the chloride was not taken into account in ion-pairing because its source is hard to determine. This may result in a minor uncertainty in  $\kappa$  calculation.”

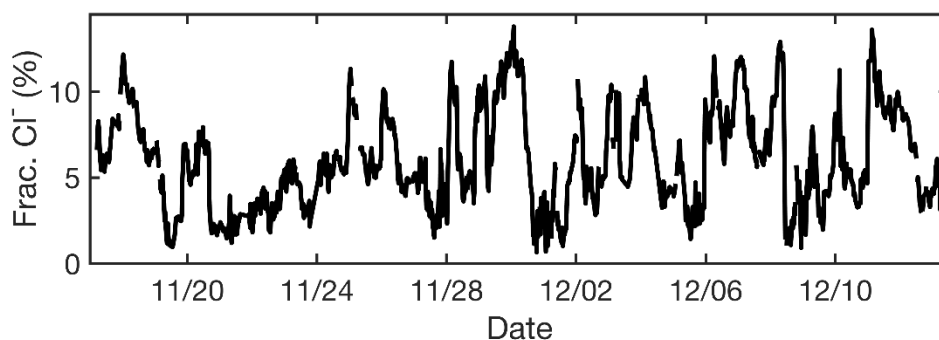


**Figure R2. The time series of the mass fraction of chloride.**

273  
274  
275  
276  
277  
278  
279  
280

Line 295: ammonium is also an important component of secondary aerosols.

Re: Good suggestion, we have added the ammonium in the line 302.

281  
282  
283  
284  
285  
286  
287  
288  
289  
290  
291  
292  
293  
294  
295  
296  
297  
298  
299  
300  
301  
302  
303  
304  
305  
306  
307  
308  
309  
  
310  
  
311  
  
312  
  
313  
  
314  
  
315  
  
316  
  
317  
  
318  
  
319  
  
320  
  
321  
  
322

**Reference:**

Bian, Y. X., Zhao, C.S., Ma, N., Chen, J., Xu, W.Y.: A study of aerosol liquid water content based on hygroscopicity measurements at high relative humidity in the North China Plain, *Atmos. Chem. Phys.*, 14 (12), 6417–6426, <https://doi.org/10.5194/acp-14-6417-2014>, 2014.

Cerully, K. M., Bougiatioti, A., Hite Jr., J. R., Guo, H., Xu, L., Ng, N. L., Weber, R., and Nenes, A.: On the link between hygroscopicity, volatility, and oxidation state of ambient and water-soluble aerosols in the southeastern United States, *Atmos. Chem. Phys.*, 15, 8679-8694, <https://doi.org/10.5194/acp-15-8679-2015>, 2015.

Guo, H., Xu, L., Bougiatioti, A., Cerully, K. M., Capps, S. L., Hite Jr., J. R., Carlton, A. G., Lee, S.-H., Bergin, M. H., Ng, N. L., Nenes, A., and Weber, R. J.: Fine-particle water and pH in the southeastern United States, *Atmos. Chem. Phys.*, 15, 5211-5228, <https://doi.org/10.5194/acp-15-5211-2015>, 2015.

Gysel, M., Grosier, J., Topping, D.O., Whitehead, J.D., Bower, J.N., Cubison, M.J., Williams, P.I., Flynn, M.J., McFiggans, G.B., Coe, H.: Closure study between chemical composition and hygroscopic growth of aerosol particles during TORCH2, *Atmos. Chem. Phys.*, 7 (24), 6131–6144, <https://doi.org/10.5194/acp-7-6131-2007>, 2007.

Kuang, Y., Zhao, C. S., Zhao, G., Tao, J. C., Xu, W., Ma, N., and Bian, Y. X.: A novel method for calculating ambient aerosol liquid water content based on measurements of a humidified nephelometer system, *Atmos. Meas. Tech.*, 11, 2967–2982, <https://doi.org/10.5194/amt-11-2967-2018>, 2018.

Sjogren, S., Gysel, M., Weingartner, E., Alfarra, M. R., Duplissy, J., Cozic, J., Crosier, J., Coe, H., and Baltensperger, U.: Hygroscopicity of the submicrometer aerosol at the high-alpine site Jungfraujoch, 3580 m a.s.l., Switzerland, *Atmos. Chem. Phys.*, 8, 5715-5729, <https://doi.org/10.5194/acp-8-5715-2008>, 2008.

Song, S., Gao, M., Xu, W., Shao, J., Shi, G., Wang, S., Wang, Y., Sun, Y., and McElroy, M. B.: Fine-particle pH for Beijing winter haze as inferred from different thermodynamic equilibrium models, *Atmos Chem Phys*, 18, 7423-7438, [10.5194/acp-18-7423-2018](https://doi.org/10.5194/acp-18-7423-2018), 2018.

Tan, H., Cai, M., Fan, Q., Liu, L., Li, F., & Chan, P. W., et al.: An analysis of aerosol liquid water content and related impact factors in pearl river delta, *Science of The Total Environment*, 579, 1822-1830, <https://doi.org/10.1016/j.scitotenv.2016.11.167>, 2017.



323  
324  
325  
326  
327  
328  
329  
330  
331  
332  
333  
334  
335  
336  
337  
338  
339  
340  
341  
342  
343  
344  
345  
346  
347  
348

# Significant contribution of organics to aerosol liquid water content in winter in Beijing, China

Xiaoai Jin<sup>1</sup>, Yuying Wang<sup>1,2</sup>, Zhanqing Li<sup>3</sup>, Fang Zhang<sup>1</sup>, Weiqi Xu<sup>4,5</sup>, Yele Sun<sup>4,5</sup>, Xinxin Fan<sup>1</sup>, Guangyu Chen<sup>6</sup>, Hao Wu<sup>1</sup>, Jingye Ren<sup>1</sup>, Qiuyan Wang<sup>2</sup>, and Maureen Cribb<sup>3</sup>

<sup>1</sup>State Key Laboratory of Earth Surface Processes and Resource Ecology, College of Global Change and Earth System Science, Beijing Normal University, Beijing 100875, China

<sup>2</sup>[Key Laboratory for Aerosol-Cloud-Precipitation of China Meteorological Administration](#), School of Atmospheric Physics, Nanjing University of Information Science and Technology, Nanjing 210044, China

<sup>3</sup>Department of Atmospheric and Oceanic Science, and Earth System Science Interdisciplinary Center, University of Maryland, College Park, MD, USA

<sup>4</sup>State Key Laboratory of Atmospheric Boundary Layer Physics and Atmospheric Chemistry, Institute of Atmospheric Physics, Chinese Academy of Sciences, Beijing 100029, China

<sup>5</sup>College of Earth Sciences, University of Chinese Academy of Sciences, Beijing 100049, China

<sup>6</sup>[Zhejiang Windey Co., Ltd., Hangzhou 310012, China](#)~~Faculty of Geographical Science, Beijing Normal University, Beijing 100875, China~~

Correspondence to: Zhanqing Li ([zli@atmos.umd.edu](mailto:zli@atmos.umd.edu)), Yuying Wang ([wyy\\_bnu@126.com](mailto:wyy_bnu@126.com))

349 **Abstract**

350

351 The aerosol liquid water content (ALWC), an important component of atmospheric particles, has a  
352 significant effect on atmospheric optical properties, visibility and multiphase chemical reactions. In  
353 this study, ALWC is determined from aerosol hygroscopic growth factor and particle number size  
354 distribution (PNSD) measurements and also simulated by the ISORROPIA II thermodynamic model  
355 with measured aerosol chemical composition data at an urban site in Beijing from 8 November to 15  
356 December 2017. Rich measurements made during the experiment concerning virtually all aerosol  
357 properties allow us not only to derive the ALWC but also to study the contributions by various species  
358 for which little has been done in this region. The simulated ALWC including the contribution of  
359 organics and the calculated ALWC are highly correlated (coefficient of determination  $R^2 = 0.92$ ). The  
360 ALWC contributed by organics ( $ALWC_{Org}$ ) accounts for  $30 \% \pm 22 \%$  of the total ALWC during the  
361 sampling period. These results suggest a significant contribution of organics to ALWC, which is rather  
362 different from previous studies that showed negligible contributions by organics. Our results also show  
363 that ALWC correlates well with the mass concentrations of sulfate, nitrate, and secondary organic  
364 aerosols (SOA) ( $R^2 = 0.66, 0.56, \text{ and } 0.60$ , respectively). We further noted that accumulation mode  
365 particles play a key role in determining ALWC, dominating among all the aerosol modes. ALWC is an  
366 exponential function of ambient relative humidity (RH) whose strong diurnal variation influence the  
367 diurnal variation of ALWC. However, there is a three-hour lag between the extremes of ALWC and  
368 RH values, due to the diurnal variations in PNSD and aerosol chemical composition. Finally, a case  
369 study reveals that  $ALWC_{Org}$  plays an important role in the formation of secondary aerosols through  
370 multiphase reactions at the initial stage of a heavy haze episode.

371

372

373

## 374 1. Introduction

375 China has experienced rapid economic developments during the past few decades, resulting in  
376 frequent heavy haze events. Severe air pollution may harm human health and affect the regional  
377 climate through aerosol direct and indirect radiation effects (Li et al., 2016; G. X. Wu et al., 2016).  
378 However, air pollution formation mechanisms and aerosol climate effects remain highly uncertain due  
379 to the complex physical and chemical processes involved (Tao et al., 2012; Y. Wang et al., 2014).

380 Aerosol liquid water (ALW), a component of atmospheric particles in the atmosphere, exists  
381 universally and plays an important role in many atmospheric physical and chemical processes (Nguyen  
382 et al., 2016). For example, ALW can influence aerosol optical properties, resulting in increased  
383 extinction coefficients, lowered atmospheric visibilities, enhanced aerosol optical depths (AODs), and  
384 changes in the direct climatic effect of aerosols (Dougle et al., 1996; Adams et al., 2001; Liao et al.,  
385 2005; Seinfeld and Pandis, 2006). Secondary aerosols (SA) are considered to be the main source of  
386 particulate pollution during heavy haze events in China (Huang et al., 2014). Many studies now  
387 highlight the significance of aerosol liquid water content (ALWC) in the formation of SA through  
388 chemical reactions (e.g., Arellanes et al., 2006; G. Wang et al., 2016; Cheng et al., 2016). This is  
389 because ALW can dilute the absolute concentration of solutes, adjust aerosol acidity, and serve as a  
390 reactant, resulting in increases in trace gas (e.g.,  $\text{N}_2\text{O}_5$  and  $\text{HO}_2$ ) uptake coefficients (Wahner et al.,  
391 1998; Bertram et al., 2009; Abbatt et al., 2012). H. Wang et al. (2017) found that the uptake coefficient  
392 of  $\text{N}_2\text{O}_5$  can be high, which is related to high ALWC in Beijing, thereby increasing the formation of  
393 nitrates. ALW can also speed up the aqueous phase chemical reaction by serving as a reactor for the  
394 transformation of  $\text{SO}_2$  to sulfate (Zheng et al., 2015; G. Wang et al., 2016; Cheng et al., 2016). Some  
395 studies have found that ALWC can facilitate the formation of secondary organic aerosols (SOA)  
396 through aqueous-phase chemistry and photochemistry (Blando et al., 2001; Surratt et al., 2007;  
397 Hennigan et al., 2008; Song et al., 2019). Furthermore, observations in Beijing have shown that  
398 aqueous-phase processes play a dominant role in the additional formation of oxidized SOA (Xu et al.,

399 2017). Overall, investigating the formation of SA and haze in North China requires an examination of  
400 ALWC and its factors including aerosol particle number size distribution (PNSD), aerosol chemical  
401 composition and ambient related humidity (RH) in this region.

402 However, directly measuring real-time ALWC is not feasible yet because of technical limitations,  
403 especially under high RH conditions (Kuang et al., 2018). Four indirect methods have been proposed  
404 to calculate real-time ALWC: (1) the aerosol ~~particle number size distribution (PNSD)~~ under dry  
405 conditions and ambient ~~relative humidity (RH)~~ conditions are first measured, then ALWC is calculated  
406 as the difference between dry and ambient aerosol volumes (Stanier et al., 2004); (2) the increased  
407 aerosol volume due to water uptake (i.e., ALWC) is calculated according to the measured dry PNSD,  
408 size-dependent aerosol hygroscopicity, and ambient RH (Kitamori et al., 2009; Bian et al., 2014; Tan  
409 et al., 2017); (3) the dry and ambient aerosol volumes are first estimated using the measured aerosol  
410 optical enhancement and Ångström exponent, then ALWC is calculated as the difference between dry  
411 and ambient aerosol volumes (Kuang et al., 2018); and (4) ALWC is simulated using thermal  
412 equilibrium models such as the ISORROPIA thermodynamic model (Nenes et al., 1998), Aerosol  
413 Inorganics Model models (Wexler and Clegg, 2002), the Simulating Composition of Atmospheric  
414 Particles in Equilibrium model (Kim et al., 1993), and the Gibb's Free Energy Minimization model  
415 (Ansari et al., 1999) with aerosol chemical composition information as input.

416 ALWC mostly depends on aerosol PNSD, chemical composition, and ambient RH. Hodas et al.  
417 (2014) reported that ALWC in the Po Valley in Italy is-was driven by locally formed anthropogenic  
418 nitrates. The implications for the lifetimes of water-soluble organic compounds and its potential  
419 influence on SOA formation were also discussed. Another study also revealed that ALWC in Beijing  
420 was driven by secondary inorganic aerosols (SIA; Z. Wu et al., 2018). Most previous studies have  
421 focused on the interaction between inorganic salts and ALWC, but the impact of organic species on  
422 ALWC been ignored to our knowledge (Blando et al., 2001; Surratt et al., 2007; Hennigan et al., 2008;  
423 Carlton et al., 2014). A thorough understanding of the association of ALWC with organic aerosols in

424 the atmosphere is lacking.

425 In this study, ALWC is calculated using the indirect method (2) and simulated using the  
426 ISORROPIA II model, i.e., indirect method (4), discussed previously. The effects of inorganic aerosols,  
427 organic aerosols, PNSD, and ambient RH on ALWC are then investigated separately. We demonstrate  
428 the significant contribution of organics to ALWC in Beijing and provide evidence that the ALW  
429 contributed by organics serves as a reactor for sulfate and SOA formation.

## 430 **2. Data and measurements**

### 431 **2.1. Sampling site**

432 The Air Pollution and Human Health (APHH) winter field campaign took place from 8 November  
433 to 15 December 2016 at the Chinese Academy of Sciences' Institute of Atmospheric Physics Tower  
434 Branch in Beijing. Beijing is located in the northwest part of the North China Plain, which has  
435 experienced rapid economic developments during the last few decades. A large amount of gaseous  
436 precursors and other air pollutants are emitted in this region every year, causing serious air pollution  
437 problems. The sampling site is located in the northwestern urban area of Beijing (39.97°N, 116.37°E),  
438 between the north third and fourth ring roads and surrounded by restaurants. Traffic and cooking  
439 emissions are thus the main pollutants at the site. Aerosols at this site can, therefore, well represent  
440 anthropogenic aerosols in highly polluted areas. Sun et al. (2013) and Y. Wang et al. (2017) provide  
441 more detailed descriptions of the sampling site.

### 442 **2.2. Instrumentation**

443 Sampling instruments used during the field campaign included a scanning mobility particle sizer  
444 (SMPS) equipped with a long differential mobility analyzer (DMA; model 3081A, TSI) and a  
445 condensation particle counter (CPC; model 3772, TSI). A custom-built hygroscopicity tandem  
446 differential mobility analyzer (H-TDMA) was installed in an air-conditioned mobile container at

447 ground level. The temperature inside the container was maintained at 20–25°C. A high-resolution  
448 aerosol mass spectrometer (HR-AMS) was set up in a sampling room located on a two-story roof,  
449 about 25 m north from the container. Sampled air went through a PM<sub>2.5</sub> cyclone inlet fixed on the top  
450 of the container before entering the instruments. The RH of the sampled air was dried to below 20 %  
451 by a dryer system consisting of a tube filled with silica gel and a Nafion dryer (model PD-70T-24ss,  
452 Perma Pure Inc., USA). Various meteorological parameters, including wind speed (WS), wind  
453 direction (WD), temperature (*T*), and RH, were measured from a 325-m meteorological tower located  
454 ~20 m west of the container. In this study, all times are reported in Beijing local time (UTC+8 h).

455 PNSDs with electrical-mobility diameters ranging from 10 to 600 nm were measured by a  
456 scanning mobility particle sizer (SMPS) at a 5-min time resolution. PNSDs were extended to diameters  
457 ranging from 0.6 to 1 μm by fitting the measured PNSDs with functions consisting of three-mode log-  
458 normal distributions (Hussein et al., 2005). Thus generated are PNSDs with a diameter range of 10 nm  
459 to 1 μm.

460 The H-TDMA system developed by the Guangzhou Institute of Tropical and Marine Meteorology  
461 measured the size-dependent aerosol hygroscopic growth factor (GF). The H-TDMA system mainly  
462 consists of four parts. The first part is a Nafion dryer to keep the RH of sampled air below 20 % and a  
463 bipolar neutralizer (soft X-ray, model 3088, TSI Inc.) to equilibrate the particle charge (Wiedensohler  
464 et al., 1988). Next, the sampled air passes through the first differential mobility analyzer (DMA1;  
465 model 3081L, TSI Inc.) to produce mono-dispersed particles. In this study, the diameters were set to  
466 40, 80, 110, 150, and 200 nm. The sampled air then went through a Nafion humidifier (model PD-70T-  
467 24ss, Perma Pure Inc., USA) used to humidify the RH of sampled air to 90 %. The last part of the H-  
468 TDMA is the second DMA (same model as the DMA1) and a water-based condensation particle  
469 counter (model 3787, TSI Inc.), used to measure the number size distribution of humidified particles  
470 in the five selected diameters. Y. Wang et al. (2017) provide a detailed introduction to the H-TDMA  
471 system.



472 Size-resolved non-refractory sub-micron aerosol chemical species, including organics (Org),  
 473 sulfate ( $\text{SO}_4^{2-}$ ), nitrate ( $\text{NO}_3^-$ ), ammonium ( $\text{NH}_4^+$ ), and chloride ( $\text{Cl}^-$ ), were measured by the HR-AMS.  
 474 The sampled air dried by diffusion silica gel dryers was drawn into the HR-AMS through a  $\text{PM}_{2.5}$   
 475 cyclone inlet to remove coarse particles larger than  $2.5 \mu\text{m}$ . The HR-AMS was calibrated with pure  
 476 ammonium nitrate following the procedures detailed in Jimenez et al. (2003). Sun et al. (2016b)  
 477 provide operational details about the HR-AMS.

### 478 3. Method

#### 479 3.1. ALWC calculation based on H-TDMA measurements

480 The ALWC is calculated based on measurements of the aerosol GF and particle number size  
 481 distribution. Briefly, H-TDMA data are first used to derive the size-resolved particle GFs at various  
 482 RHs. Then ALWC is calculated as the increased aerosol volume due to hygroscopic growth attributed  
 483 to water uptake.

484 Chen et al. (2012) ~~show~~showed how to calculate size-resolved particle GFs at different RHs. First,  
 485 a three-mode log-normal distribution is applied to fit the measured PNSD to produce fitting parameters  
 486 for each mode. The hygroscopicity parameter ( $\kappa$ ) in any mode is assumed to be constant. The H-  
 487 TDMA-derived size-dependent  $\kappa$  can then be used to deduce the corresponding  $\kappa$  for the nucleation  
 488 mode, the Aitken mode, and the accumulation mode of PNSDs according to the following equation:

$$489 \quad \kappa(D_p) = \frac{\sum_{i=1}^3 \kappa_i \cdot N_i(D_p)}{\sum_{i=1}^3 N_i(D_p)}, \quad (1)$$

490 where  $\kappa_i$  refers to the  $\kappa$  of the  $i$ th mode, and  $N_i(D_p)$  refers to the number concentration of particles in  
 491 the  $i$ th mode. According to  $\kappa$ -Köhler theory (Petters and Kreidenweis, 2007),  $\kappa$  at a certain diameter  
 492 ( $D_d$ ) can be calculated as

$$493 \quad \kappa(D_d) = (\text{GF}^3 - 1) \cdot \left[ \frac{1}{\text{RH}} \exp\left(\frac{4\sigma_s/aM_w}{RT\rho_w D_d \text{GF}}\right) - 1 \right], \quad (2)$$

494 where RH is the control value by the humidifier in the H-TDMA system,  $T$  is the mean room

495 temperature of the container set to 293 K,  $\sigma_{s/a}$  is the surface tension of the solution/air interface assumed  
 496 to be the same as the surface tension coefficient between water and air (about 0.0728 N m<sup>-1</sup> at 293 K),  
 497  $M_w$  is the molecular weight of water,  $R$  is the universal gas constant,  $\rho_w$  is the density of water, and  $D_d$   
 498 is the diameter of the dry particles. The GF at a given RH is defined as the ratio of the humidified  
 499 diameter [ $D_p$  (RH)] to  $D_d$ :

$$500 \quad \text{GF} = D_p(\text{RH})/D_d . \quad (3)$$

501 The known  $\kappa$  of each mode derives the size-resolved  $\kappa$  at 90 % RH using Eq. (1). Substituting the size-  
 502 resolved  $\kappa$  into Eq. (2) results in size-resolved GFs at various RHs. Finally, the volume of ALWC at  
 503 ambient RH is equal to the increased aerosol volume due to water uptake, i.e., ALWC can be calculated  
 504 as

$$505 \quad \text{ALWC}_{\text{HTDMA}} = \left[ \frac{1}{6} \sum_i n_i D_{p,i}^3 \left( \text{GF}(D_{p,i}, \text{RH})^3 - 1 \right) \right] \cdot \rho_w , \quad (4)$$

506 where  $n_i$  refers to the particle number concentration of dry particles for the corresponding particle size  
 507 range in the  $i$ th mode, and  $D_{p,i}$  refers to the particle diameter for the corresponding particle size range.

### 508 **3.2. ALWC simulations based on the ISORROPIA II model**

509 The thermodynamic equilibrium model ISORROPIA II developed by Fountoukis and Nenes  
 510 (2007) using aerosol chemical composition information from the HR-AMS can simulate ALWC  
 511 (ALWC<sub>ISO</sub>). The bulk chemical composition was used in the model. However, the ISORROPIA II  
 512 model only considers the contribution of inorganic species (Ca<sup>2+</sup>, K<sup>+</sup>, Mg<sup>2+</sup>, NH<sup>+</sup>, Na<sup>+</sup>, SO<sub>4</sub><sup>2-</sup>, NO<sub>3</sub><sup>-</sup>,  
 513 Cl<sup>-</sup> and H<sub>2</sub>O) on ALWC and neglects the contribution of organics. In this study, the phase state was  
 514 assumed to be stable in the model calculation, and the model was set up to reverse mode due to the  
 515 lack of measurements of gaseous ammonia.

516 According to the model assumptions that the aerosol curvature effect in Köhler theory is ignored,  
 517 and the aerosol water uptake has no effect on ambient vapor pressure, the water activity ( $a_w$ ) defined  
 518 as the effective mole fraction of water is equal to the ambient RH in this model (Seinfeld and Pandis,

519 2006):

$$520 \quad a_w = RH \quad (5)$$

521 The ALWC can be calculated using the Zdanovskii–Stokes–Robinson (ZSR) mixing rule (Stokes and  
522 Robinson, 1966),

$$523 \quad ALWC_{ISO} = \sum_i \frac{M_i}{m_{0i}(a_w)}, \quad (6)$$

524 where  $M_i$  is the mole concentration of the  $i$ th species ( $\text{mol m}^{-3}$  in air), and  $m_{0i}(a_w)$  is the corresponding  
525 molality of the binary solution of the  $i$ th species under the same  $a_w$  with complex solution. Finally,  
526 with measured ambient RH and  $T$  values as input  $ALWC_{ISO}$  values under different RH and  $T$  conditions  
527 can be derived.

### 528 3.3. Inferring the contribution of organics to ALWC

529 According to the  $\kappa$ -Köhler theory and the ZSR mixing rule,  $\kappa$  can also be expressed as the sum of  
530 the contributions of each aerosol component:

$$531 \quad \kappa = \sum_i \varepsilon_i \kappa_i, \quad (7)$$

532 where  $\varepsilon_i$  and  $\kappa_i$  are the volume fraction and hygroscopicity of the  $i$ th species, respectively. Submicron  
533 aerosols mainly consist of organic and inorganic species (Carbone et al., 2013; Zieger et al., 2017). As  
534 mentioned in section 2.2, the HR-AMS measures the mass concentrations of organics and inorganics,  
535 including  $\text{SO}_4^{2-}$ ,  $\text{NO}_3^-$ ,  $\text{NH}_4^+$ , and  $\text{Cl}^-$ . The volume fraction of inorganic species can be calculated based  
536 on the ion-pairing scheme given by the following equations (Gysel et al., 2007):

$$\begin{aligned} 537 \quad n_{\text{NH}_4\text{NO}_3} &= n_{\text{NO}_3^-}, \\ 538 \quad n_{\text{NH}_4\text{HSO}_4} &= \min(2n_{\text{SO}_4^{2-}} - n_{\text{NH}_4^+} + n_{\text{NO}_3^-}, n_{\text{NH}_4^+} - n_{\text{NO}_3^-}), \\ 539 \quad n_{(\text{NH}_4)_2\text{SO}_4} &= \max(n_{\text{NH}_4^+} - n_{\text{NO}_3^-} - n_{\text{SO}_4^{2-}}, 0), \\ 540 \quad n_{\text{H}_2\text{SO}_4} &= \max(0, n_{\text{SO}_4^{2-}} - n_{\text{NH}_4^+} + n_{\text{NO}_3^-}), \\ 541 \quad n_{\text{HNO}_3} &= 0, \end{aligned} \quad (8)$$

542 where  $n$  represents the mole numbers, and “min” and “max” are minimum and maximum values,  
543 respectively. The  $\kappa$  values of the inorganic species sulfuric acid, ammonium sulfate, ammonium  
544 hydrogen sulfate, and ammonium nitrate are 1.19, 0.48, 0.56, and 0.58, respectively (Topping et al.,  
545 2005; Petters and Kreidenweis, 2007). So the ZSR model can be used to estimate the contribution of  
546 inorganic species to the  $\kappa$  value. In this paper, the chloride was not taken into account in ion-pairing  
547 because its source is hard to determine. This may result in a minor uncertainty in  $\kappa$  calculation. The  
548 hygroscopicity parameter of organics ( $\kappa_{Org}$ ) can be calculated using the volume fraction of organics  
549 and the total  $\kappa$  value derived from the H-TDMA, according to Eq. (7). Finally, the ALWC contributed  
550 by organic species ( $ALWC_{Org}$ ) can be calculated as (Petters and Kreidenweis, 2007)

$$551 \quad ALWC_{Org} = \frac{m_{Org} \rho_W}{\rho_{Org}} \frac{\kappa_{Org}}{\left(\frac{1}{RH} - 1\right)}, \quad (9)$$

552 where  $m_{Org}$  is the organic mass concentration from the AMS (Xu et al., 2015), and  $\rho_{Org}$  is the density  
553 of organics, taken as  $1.4 \text{ g cm}^{-3}$  (Moore et al., 2011; Lathem et al., 2013; Cerully et al., 2014).

## 554 4. Results and discussion

### 555 4.1. Comparison of calculated and simulated ALWC

556 The trends in ALWC calculated based on the hygroscopic growth factor and PNSD  
557 ( $ALWC_{HTDMA}$ ) and simulated from ISOPPOPIA II model ( $ALWC_{ISO}$ ) are generally consistent ~~(Fig.~~  
558 ~~S1). However, the difference between  $ALWC_{HTDMA}$  and  $ALWC_{ISO}$  is large at low RH, especially at~~  
559 ~~ultra-low RH ( $< 30\%$ ).~~ Figure 1a shows that  $ALWC_{HTDMA}$  and  $ALWC_{ISO}$  agree well and that their  
560 coefficient of determination ( $R^2$ ) is 0.89. The correlation is especially strong for RH over 90 %.  
561 However, for RH below 60 %,  $ALWC_{ISO}$  is less than  $ALWC_{HTDMA}$  and even close to 0 in some cases.  
562 Bian et al. (2014) and Tan et al. (2017) observed a similar phenomenon in northern and southern China.  
563 There are ~~two~~ three possible explanations for these results. H-TDMA samples were humidified to 90 %  
564 RH during the field campaign, thereby leading to the neglect of the deliquescence process in the  
565  $ALWC_{HTDMA}$  calculation. This may lead to overestimation of  $ALWC_{HTDMA}$  for RH below the

566 deliquescence relative humidity (DRH). Second, the assumption of constant  $\kappa$  in each mode may lead  
567 to small uncertainty in size-resolved GFs at different RHs, resulting in small deviation in ALWC  
568 calculation. This may be another reason for the difference between  $ALWC_{HTDMA}$  and  $ALWC_{ISO}$ . In  
569 addition, the ISORROPIA II model ignores the effect of aerosol shape and complex organic species  
570 on the DRH. Previous studies have suggested that the particle spherical assumption and simplified  
571 aerosol chemical species in this model can overestimate the DRH (Seinfeld and Pandis, 2006; Sjogren  
572 et al., 2007). So for RH below the simulated DRH (~60 %), particles may still be dry in the  
573 ISORROPIA II model, but may have been hydrated in the real atmosphere. Therefore, this model  
574 underestimates ALWC. The ambient aerosol deliquescent phenomenon is rare in the North China Plain  
575 (Kuang et al., 2016). In addition, the ISORROPIA II model cannot simulate water uptake by organics,  
576 which can lead to some bias between simulated and calculated ALWCs. As described in section 3.3,  
577  $ALWC_{Org}$  can be inferred and used to discuss differences between  $ALWC_{ISO}$  and  $ALWC_{HTDMA}$ . Figure  
578 1b shows that adding  $ALWC_{Org}$  to  $ALWC_{ISO}$  leads to a stronger correlation with  $ALWC_{HTDMA}$  ( $R^2 =$   
579 0.92). The correlation improves significantly for RH below 60 %. This demonstrates that (1) organic  
580 species contribute significantly to ALWC, and (2) the underestimation of ALWC by the ISORROPIA  
581 II model is also related to the neglect of organic species in the model.

582

## 583 **4.2. Impact of different factors on ALWC**

### 584 **4.2.1. Impact of aerosol chemical species on ALWC**

585 Figure 2 shows the characteristics of seven heavy pollution events selected for examination.  
586 Figures 2a and 2c display the time series of WS, WD, and ambient RH. The prevailing wind during  
587 the haze episodes was a weak southerly wind that was favorable for bringing in pollutants from the  
588 highly populated and industrialized neighboring regions to the sampling site. This is beneficial to the  
589 formation and accumulation of SA (T. Wang et al., 2010; Y. Wang et al., 2017). However, the prevailing

590 winds during the clean events were strong northerly winds that always carried in a clean air mass,  
591 resulting in pollutants being quickly removed (Figure 2c). Note that the  $PM_{10}$  mass concentration  
592 decreases somewhat in the evening during haze episodes, following the short-term change of WD from  
593 southerly to northerly. This is related to mountain-valley breezes in Beijing (Wehner et al., 2008; Gao  
594 et al., 2011; Y. Wang et al., 2017). These results demonstrate that heavy haze episodes have a strong  
595 correlation with local wind direction in Beijing.

596 Figures 2a and 2d show the time series of ambient RH and mass concentrations of aerosol chemical  
597 species in  $PM_{10}$ . These figures suggest that the increase in inorganic and organic aerosols is  
598 synchronous with the increase in ambient RH during the heavy pollution periods (P1-P7). This is likely  
599 because of a positive feedback mechanism driven by Henry's law and thermodynamic equilibrium (Z.  
600 Wu et al., 2018). Figure 2b also shows that ALWC continuously increases during the pollution  
601 accumulation period. On average, ALWC increases from 8 to  $89 \mu g m^{-3}$  as ambient RH increases from  
602 15 to 80 %, and the inorganic and organic aerosol mass concentrations increase from 15 to  $120 \mu g m^{-3}$   
603 and from 12 to  $78 \mu g m^{-3}$ , respectively. These results imply that the increase in ambient RH and  
604 aerosol mass concentration are all important for the increase in ALWC.

605 Equation (4) also suggests that the absolute value of ALWC is dependent on the value of ambient  
606 RH and aerosol chemical composition (i.e., the GF value). To further investigate the impact of  
607 chemical composition on ALWC, the impact of RH on ALWC should be accounted for. Previous  
608 studies suggest there is an exponential relationship between ALWC and RH (e.g., Z. Wu et al., 2018).  
609 Here, we define the relative ALWC as the ratio of  $ALWC_{HTDMA}$  and the function of ambient RH ( $e^{bRH}$ ).

610 The b is derived according to the relationship between  $ALWC_{HTDMA}$  and RH that is fitted by the  
611 function  $y = ae^{bx}$ . Figure 3a shows the relationship between relative ALWC and primary aerosols  
612 (PA) or SA mass concentrations. PA consists of primary organic aerosols (POA) and black carbon  
613 (BC), and SA consists of SOA, sulfate, and nitrate. The positive matrix factorization (Paatero and  
614 Tapper, 1994) was applied on the organic aerosols (OA) spectral matrices to identify POA and SOA.



615 The relative ALWC is highly correlated with SA mass concentrations ( $R^2 = 0.94$ ) but poorly correlated  
616 with PA mass concentrations ( $R^2 = 0.69$ ). High relative ALWCs coincident with high SA mass  
617 concentrations suggest that SA plays a key role in the increase in ALWC. This is likely because SA is  
618 mainly generated from photochemical reactions in the daytime or reactions at night, making SA highly  
619 aged with a hygroscopicity stronger than that of PA (Ervens et al., 2011; Sareen et al., 2017). SA can,  
620 therefore, absorb more water vapor than PA in the atmosphere. The enhanced aerosol liquid water  
621 induced by SA is further favorable for the formation of SA by speeding up the atmospheric chemical  
622 reaction rate and serving as the medium for gas-particle heterogeneous reactions (G. Wang et al., 2016;  
623 Cheng et al., 2016). This further increases the bulk aerosol hygroscopicity. This is also the reason why  
624 inferred  $\kappa$  based on the ZSR model continuously increases during haze episodes (Figure 2c).

625 Secondary aerosols are mainly composed of nitrate, sulfate, ammonium and SOA. To determine  
626 which species is the driver for ALWC in Beijing, Figure 3b shows the correlation analysis between  
627 relative ALWC and the mass concentrations of different aerosol chemical species. Relative ALWC and  
628 all SIA agree well [ $R^2$  equal to 0.66 (sulfate) and 0.56 (nitrate)]. It has been reported that ALWC is  
629 driven by inorganic salts with both nitrate and sulfate playing key roles in determining ALWC (Z. Wu  
630 et al., 2018). ALWC also agrees well with SOA ( $R^2 = 0.60$ ) in our study. This is unexpected because  
631 the hygroscopicity of SOA is relatively lower than that of nitrate and sulfate. Some studies have also  
632 suggested that the water uptake of aged organics accounts for only a few percent of the total aerosol  
633 water uptake (e.g., Gysel et al., 2007; Engelhart et al., 2011). In our study, the contribution of  $ALWC_{Org}$   
634 to total ALWC is significant, accounting for  $30\% \pm 22\%$ . As shown in Figure 4, the contribution of  
635 organics to total ALWC varies strongly. This is likely related with the variation in mass fraction and  
636 hygroscopicity parameter of organics ( $\kappa_{Org}$ ). The mass concentration of inorganics increases more than  
637 that of organics as RH increases, leading to a lower mass fraction of organics in the case of high  
638 ambient RH. Figure 4 also shows  $ALWC_{Org}$  fraction increases significantly with the increase of  $\kappa_{Org}$ .  
639 All these help explain a large variation in the  $ALWC_{Org}$  contribution to total ALWC. Considering the

640 distinct ambient RH and  $\kappa_{\text{org}}$  between clean and polluted periods, we calculated respectively the  
641 fraction of  $\text{ALWC}_{\text{Org}}$  during two periods. There is a higher  $\text{ALWC}_{\text{Org}}$  fraction ( $33\% \pm 23\%$ ) during  
642 clean periods than that during polluted periods ( $26\% \pm 11\%$ ). Yet, there is little variability of  $\text{ALWC}_{\text{Org}}$   
643 fraction during polluted periods. The larger variability in  $\text{ALWC}_{\text{Org}}$  fraction during clean periods is  
644 likely caused by the highly variable  $\kappa_{\text{org}}$  when the ambient RH is low. In summary, the contribution of  
645 organics in total ALWC varies with the variations of the mass fraction of organics and  $\kappa_{\text{org}}$ , and this  
646 contribution is significant during both clean and polluted periods. Studies of ALWC in Beijing,  
647 therefore, cannot neglect  $\text{ALWC}_{\text{Org}}$ . This is different from the studies in other regions such as in the  
648 Po Valley in Italy (Hodas et al., 2014) and the eastern U.S. (Carlton et al., 2013) where the ALWC was  
649 found to be only driven by nitrate and sulfate respectively.

650 An interesting phenomenon is frequently observed at the initial stage of heavy haze episodes (e.g.,  
651 P4, P5, P6, and P7).  $\text{ALWC}_{\text{ISO}}$  is almost close to 0, but both  $\text{ALWC}_{\text{HTDMA}}$  and  $\text{ALWC}_{\text{Org}}$  are always  
652 larger than 0, and the organic aerosol mass fraction is high at this stage. These observations reveal that  
653 at the initial stage of heavy haze episodes, the ALWC is mostly contributed by organic species.  
654 Meanwhile,  $\kappa$  is not very low and increases markedly as the  $\text{PM}_{10}$  mass concentration increases, which  
655 is unexpected because of the lower hygroscopicity of organic aerosols compared to SIA. Therefore,  
656 some highly hygroscopic substance (i.e., SA) must be generated through multiphase chemical reaction  
657 at this stage. We propose that the liquid water contributed by organic species provides a reactor for the  
658 transformation of gaseous precursors to SA at the initial stages of heavy haze episodes, increasing the  
659 uptake of more liquid water by more SA and further accelerating the formation of heavy haze. Section  
660 4.3 provides a case study to demonstrate this.

#### 661 **4.2.2. Impact of PNSD on ALWC**

662 In addition to aerosol chemical composition, ALWC also depends on PNSD (Bian et al., 2014).  
663 As described in section 3.1, the nucleation mode ( $< 30$  nm), the Aitken mode (30–110 nm), and the  
664 accumulation mode (110 nm to 1  $\mu\text{m}$ ) (Whitby, 1978; Birmili et al., 2001) are considered in this study.

665 Particles with diameters greater than 1  $\mu\text{m}$  are not considered because ~~most of these large particles are~~  
666 ~~composed of hydrophobic species (e.g., dust or mineral substances) that contribute little to ALWC~~  
667 ~~some particles in the coarse mode are water soluble but their contribution on the ALWC is low (e.g.,~~  
668 ~~Hussein et al., 2004; S. Liu et al., 2008; Bian et al., 2014; Tan et al., 2017).~~

669 Figure [5S2](#) in the supplement shows that the contributions of nucleation mode, Aitken mode, and  
670 accumulation mode particles to ALWC are < 1.0 %, 18.0 %, and 82.0 %, respectively. Figure [64](#) shows  
671 the correlations between  $\text{ALWC}_{\text{HTDMA}}$  and the volume concentrations of different mode particles, and  
672 the average contribution of different mode particles to  $\text{ALWC}_{\text{HTDMA}}$  ( $f_{\text{ALWC}}$ ) under five different RH  
673 conditions. The  $R^2$  and  $f_{\text{ALWC}}$  of the nucleation mode particles (left column in Figure [64](#)) are all less  
674 than 0.1 and 1 %, respectively, under all RH conditions. This is likely because the volume  
675 concentration of nucleation mode particles is very low, and most of these small particles are composed  
676 of hydrophobic chemical species such as BC and POA. Similarly, the number concentration of Aitken  
677 mode particles also shows weak correlations with  $\text{ALWC}_{\text{HTDMA}}$  ( $R^2 < 0.2$ ) under  $\text{RH} < 90\%$  conditions,  
678 but their correlation ( $R^2 = 0.25$ ) is enhanced significantly under  $\text{RH} > 90\%$  conditions (middle column  
679 of Figure [64](#)). This is because there are more aged particles in the Aitken mode which can absorb much  
680 more water when the ambient RH is higher than 90 %. However, the contribution of the Aitken mode  
681 to ALWC ranges from 14 % to 21 % and decreases as RH increases.  $\text{ALWC}_{\text{HTDMA}}$  is strongly correlated  
682 to the volume concentration of accumulation mode particles, with  $R^2$  and  $f_{\text{ALWC}}$  greater than 0.6 and  
683 75 %, respectively, under all RH conditions (right column of Figure [64](#)). Figure [64](#) also shows that  
684 ALWC increases slightly as the volume concentration of accumulation mode particles increases under  
685  $\text{RH} < 70\%$  conditions (slope < 0.001), but increases strongly under higher RH conditions, especially  
686 under  $\text{RH} > 90\%$  conditions (slope = 0.0041). This is likely because there are more accumulation  
687 mode SA formed due to multiphase chemical reactions under high ambient RH conditions. Swietlicki  
688 et al. (1999) have suggested that the contribution of accumulation mode particles to ALWC is largest  
689 for all-mode particles.

690 In summary, the contribution of nucleation mode particles to ALWC is very low. The contribution  
691 of Aitken mode particles is much higher than nucleation mode particles and decreases with increasing  
692 ambient RH. The contribution of accumulation mode particles to ALWC is largest under all RH  
693 conditions and increases with increasing ambient RH, thus playing a key role in determining ALWC.

### 694 4.2.3. Impact of RH on ALWC

695 As discussed in 4.2.1, the absolute value of ALWC has an exponential relationship with ambient  
696 RH. Figure 75 shows the relationship between ALWC and RH for different PM<sub>1</sub> mass concentration  
697 ranges. ALWC increases slowly as RH increases under lower ambient RH conditions then sharply  
698 increases when RH exceeds a critical RH value. This critical RH value is different for different PM<sub>1</sub>  
699 mass concentrations. This is because the low RH conditions cannot provide enough water for aerosol  
700 particles, even though the PNSD is dominated by accumulation mode particles with higher  
701 hygroscopicity (Tan et al., 2016). This demonstrates the important influence of RH on ALWC. The  
702 lower critical RH value for higher PM<sub>1</sub> mass concentrations (~80 %) suggests that ALWC is easily  
703 formed under heavily polluted conditions. This is likely because there are more SA and accumulation  
704 mode particles during pollution periods (Sun et al., 2016a; Y. Wang et al., 2017).

705 Figure 86a shows the diurnal variations of ALWC<sub>HTDMA</sub> and ambient RH during the sampling  
706 period. The extreme ALWC<sub>HTDMA</sub> values appear at night and during the day respectively, likely related  
707 to the diurnal variations of ambient RH. The elevated ambient RH at night not only increases ALWC  
708 through water uptake of particles directly, but also facilitates the formation of hydrophilic particulate  
709 nitrate through the speeding up of the uptake coefficient of N<sub>2</sub>O<sub>5</sub> (Thornton et al., 2003; Bertram et  
710 al., 2009). This can further enhance ALWC. However, although the diurnal variations of ALWC<sub>HTDMA</sub>  
711 and ambient RH are similar, the peak and nadir of ALWC<sub>HTDMA</sub> (0300 LT and 1100 LT, respectively)  
712 appear three hours earlier than the peak and nadir of ambient RH (0600 LT and 1400 LT, respectively).  
713 This time difference is likely related to changes in PNSD. The diurnal variation of PNSD (Figure 86b)  
714 shows that the number concentrations of Aitken and accumulation mode particles begin to decrease

715 quickly at 0300 LT. ALWC also begins to decrease, although the ambient RH increases slightly at that  
716 time. In the morning, ALWC decreases sharply following the ambient RH and PNSD changes due to  
717 the lifting planetary boundary layer height. ALWC decreases to its minimum value at ~1100 LT then  
718 begins to increase quickly. However, ambient RH still decreases at that time and reaches its minimum  
719 value at ~1400 LT. The increase in ALWC is likely associated with changes in aerosol chemical species  
720 and PNSD. Figure 86b and 86c show that there are many newly formed Aitken and accumulation mode  
721 particles and that the fraction of SA increases at noon, likely because of strong photochemical  
722 reactions. Y. Wang et al. (2017, 2018) have suggested that daytime photochemical reactions are  
723 efficient enough to enhance aerosol hygroscopicity and change the aerosol mixing state from external  
724 to internal in North China through the formation of hydrophilic chemical species. All this suggests that  
725 ambient RH is not the only determining factor for ALWC. PNSD and aerosol chemical composition  
726 are also important for ALWC.

### 727 4.3. A case study of the impact of $ALWC_{Org}$ on SA formation

728 As discussed in section 4.2.1, a hypothesis is proposed that  $ALWC_{Org}$  maybe provide a reactor for  
729 the formation of secondary species. To verify this hypothesis, the P4 case shown in Figure2 is selected  
730 to further analyze the influence of  $ALWC_{Org}$  on the formation of secondary aerosols (Figure 97). Figure  
731 97a shows the time series of  $ALWC_{HTDMA}$ ,  $ALWC_{ISO}$ , and  $ALWC_{Org}$  during this case. On 27 November  
732 2017,  $ALWC_{ISO}$  was close to 0 all day long because of the low ambient RH, but both  $ALWC_{HTDMA}$  and  
733  $ALWC_{Org}$  were always larger than 0, increasing with increasing  $PM_{10}$  mass concentration (Figure 97a).  
734 Figure 9a7a also shows that the fraction of  $ALWC_{Org}$  in  $ALWC_{HTDMA}$  was high at the initial stage of  
735 this pollution case, but this fraction decreased as haze increased. This case was further divided into  
736 three periods (Figure 97b). Organics were the most abundant chemical species during the first period  
737 (64 %), which explains the high fraction of  $ALWC_{Org}$  in  $ALWC_{HTDMA}$  at the initial stage of this haze  
738 case. The pie charts in Figure 97b also show that both SOA and SIA (sulfate, nitrate, and ammonium)  
739 increases from the first to third periods but POA decreases, likely related to multiphase reactions (i.e.,

740 aqueous-phase reactions) due to the enhanced ALWC. Time series of  $f_{44}$  and the fraction of sulfate in  
741 total sulfur ( $F_{\text{SO}_4^{2-}}$ ) are also shown to further illustrate the influence of aqueous-phase reactions on  
742 aerosol chemical species. The  $m/z$  44 signal intensity  $f_{44}$  (mostly contributed by the  $\text{CO}_2^+$  ion) measured  
743 by the AMS can be used as an indicator of the oxidation level in organic species (Mei et al., 2013).  
744 The sulfur oxidation ratio  $F_{\text{SO}_4^{2-}}$  (Sun et al., 2006) is defined as

$$745 \quad F_{\text{SO}_4^{2-}} = \frac{n[\text{SO}_4^{2-}]}{n[\text{SO}_4^{2-}] + n[\text{SO}_2]}, \quad (10)$$

746 where  $n[\text{SO}_4^{2-}]$  and  $n[\text{SO}_2]$  refer to the molar concentrations of  $\text{SO}_4^{2-}$  and  $\text{SO}_2$ , respectively. Figure  
747 [97b](#) suggests that  $f_{44}$  and  $F_{\text{SO}_4^{2-}}$  both increase gradually with increasing  $\text{ALWC}_{\text{HTDMA}}$  and  $\text{PM}_{10}$  mass  
748 concentration from 27 November to 30 November 2017. This is likely because the increase in ALWC  
749 is beneficial to the oxidation of organics and the transformation of  $\text{SO}_2$  to  $\text{SO}_4^{2-}$ , implying the  
750 importance of aqueous-phase chemical reaction on haze formation in Beijing. The production of  
751 secondary organic and inorganic species can further enhance aerosol hygroscopicity, increasing ALWC  
752 in the atmosphere. This positive feedback is the reason behind the rapid formation of heavy haze events  
753 in Beijing (G. Wang et al., 2016). A rapid increase in  $f_{44}$  and  $F_{\text{SO}_4^{2-}}$  was seen during the first period at  
754 night on 27 November (shown by green and red arrows in Fig. [97](#)) when organics contributed the most  
755 to ALWC. This suggests that ALWC contributed by organics may have played an important role in the  
756 formation of secondary species at the initial stage of the pollution event.

757

## 758 5. Conclusions

759 In this study, the aerosol liquid water content (ALWC) was calculated using the size-resolved  
760 aerosol hygroscopic growth factor and the particle number size distribution (PNSD) measured at a  
761 Beijing urban site during the APHH winter campaign (8 November to 15 December 2017). Also done  
762 were simulations using the ISORROPIA II model with measured aerosol chemical composition data



763 as input data. During the sampling period, seven heavy haze episodes were selected to investigate the  
764 influence of different factors (PNSD, ambient RH, and aerosol chemical composition) on ALWC.

765 The calculated and simulated ALWC ( $ALWC_{HTDMA}$  and  $ALWC_{ISO}$ ) agree well (correlation of  
766 determination  $R^2$  equal to 0.89). However,  $ALWC_{ISO}$  is much lower than  $ALWC_{HTDMA}$  for RH below  
767 60 %, even approaching zero many times. This deviation is in part attributed to the neglect of the  
768 contribution of organics to ALWC ( $ALWC_{Org}$ ) in the ISORROPIA II model, contradicting with  
769 previous studies ignoring this contribution. The aerosol hygroscopicity of organics was also derived  
770 in this study for use in calculating  $ALWC_{Org}$ . The sum of  $ALWC_{ISO}$  and  $ALWC_{Org}$  has a higher  
771 correlation ( $R^2 = 0.92$ ) with the calculated ALWC (i.e.,  $ALWC_{HTDMA}$ ), especially for RH below 60 %.  
772 This implies that organic aerosols are also an important contributor to ALWC.

773 PNSD, ambient RH, and aerosol chemical composition are all found to affect ALWC significantly.  
774 Nucleation mode and Aitken mode particles have little influence on ALWC. Accumulation mode  
775 particles play a key role in determining ALWC and dominate among all aerosol modes. ALWC is  
776 highly related to the relative humidity (RH) when RH exceeds a critical RH value that is different for  
777 different  $PM_{10}$  mass concentrations. ALWC varies diurnally with its extreme values appearing at night  
778 and during the day respectively. The diurnal variation of ambient RH explains this. However, there is  
779 a three-hour difference between when the extreme ALWC and RH values occur, caused by the diurnal  
780 variations in PNSD and aerosol chemical composition.

781 On average,  $ALWC_{Org}$  accounts for  $\sim 30 \% \pm 22 \%$  of the total aerosol liquid water during the  
782 sampling period. This shows the significant contribution of organic species to ALWC. Our results  
783 suggest that ALWC is not only driven by inorganic salts but also driven by organics in Beijing. This is  
784 different from the results obtained in the Po Valley in Italy (Hodas et al., 2014) and the eastern U.S.  
785 (Carlton et al., 2013) where the ALWC is driven by nitrate and sulfate respectively. Finally, one case  
786 study was used to study the importance of  $ALWC_{Org}$  on multiphase chemical reactions.  $ALWC_{Org}$  was  
787 found to play an important role in the formation of secondary aerosols by speeding up aqueous-phase

788 reactions at the initial stage of heavy haze. Our study is important for investigating the contribution of  
789 organics to ALWC and its importance on haze formation in Beijing.

790

791 *Data availability.* Data used in the study are available from the first author upon request  
792 ([201631490012@mali.bnu.edu.cn](mailto:201631490012@mali.bnu.edu.cn)).

793

794 *Author contributions.* ZL and YW designed the experiment; YW, XJ, and WX carried it out and  
795 analyzed the data; other co-authors participated in science discussions and suggested additional  
796 analyses. XJ and YW prepared the paper with contributions from all co-authors.

797

798 *Competing interests.* The authors declare no competing interests.

799

800 *Acknowledgements.* This work was funded by the National Key R&D Program of China (grant no.  
801 2017YFC1501702), [the](#) National Natural Science Foundation of China (NSFC) research projects  
802 (grant nos. 91544217, [4157513241575143](#), 41675141, 41705125), [the Startup Foundation for](#)  
803 [Introducing Talent of NUIST](#) and the National Basic Research Program of China “973” (grant no.  
804 2013CB955801). We thank all participants of the field campaign for their tireless work and  
805 cooperation.

806

## 807 **References**

808

809 Abbatt, J. P. D., Lee, A. K. Y., Thornton, J. A.: Quantifying Trace Gas Uptake to Tropospheric Aerosol:  
810 Recent Advances and Remaining Challenges, *Chem. Soc. Rev.*, 41(19), 6555–6581,  
811 <https://doi.org/10.1039/c2cs35052a>, 2012.

812 Adams, P. J., and Seinfeld, J. H.: General circulation model assessment of direct radiative forcing by  
813 the sulfate-nitrate–ammonium–water inorganic aerosol system, *J. Geophys. Res.-Atmos.*, 106,  
814 1097–1111, <https://doi.org/10.1029/2000JD900512>, 2001.

815 Ansari, A.S., Pandis, S.N.: Prediction of multicomponent inorganic atmospheric aerosol behavior,  
816 *Atmos. Environ.*, 33 (5), 745–757, [https://doi.org/10.1016/S1352-2310\(98\)00221-0](https://doi.org/10.1016/S1352-2310(98)00221-0), 1999.

817 Arellanes, C., Paulson, S. E., Fine, P. M., and Sioutas, C.: Exceeding of Henry’s Law by Hydrogen  
818 Peroxide Associated with Urban Aerosols, *Environ. Sci. Technol.*, 40, 4859–4866,  
819 <https://doi.org/10.1021/es0513786>, 2006.

820 Bertram, T. H., Thornton, J. A.: Toward a general parameterization of N<sub>2</sub>O<sub>5</sub> reactivity on aqueous  
821 particles: the competing effects of particle liquid water, nitrate and chloride, *Atmos. Chem. Phys.*, 9  
822 (21), 8351–8363, <https://doi.org/10.5194/acp-9-8351-2009>, 2009.

823 Bian, Y.X., Zhao, C.S., Ma, N., Chen, J., Xu, W.Y.: A study of aerosol liquid water content based on  
824 hygroscopicity measurements at high relative humidity in the North China Plain, *Atmos. Chem.*  
825 *Phys.*, 14 (12), 6417–6426, <https://doi.org/10.5194/acp-14-6417-2014>, 2014.

826 Birmili, W., Wiedensohler, A., Heintzenberg, J., and Lehmann, K.: Atmospheric particle number size  
827 distribution in central Europe: Statistical relations to air masses and meteorology, *J. Geophys. Res.-*  
828 *Atmos.*, 106, 32005–32018, <https://doi.org/10.1029/2000JD000220>, 2001.

829 Blando, J. D., Turpin, B. J.: Secondary organic aerosol formation in cloud and fog droplets: a literature  
830 evaluation of plausibility, *Atmos. Environ.*, 34, 1623–1632, [https://doi.org/10.1016/S1352-  
831 \*2310\(99\)00392-1\*, 2001.](https://doi.org/10.1016/S1352-2310(99)00392-1)

832 Carbone, S., Saarikoski, S., Frey, A., Reyes, F., Reyes, P., Castillo, M., Gramsch, E., Oyola, P., Jayne,  
833 J., Worsnop, DR., and Hillamo, R.: Chemical characterization of submicron aerosol particles in  
834 Santiago de Chile, *Aerosol Air Qual. Res.*, 13(2), 462-473,  
835 <https://doi.org/10.4209/aaqr.2012.10.0261>, 2013.

836 Carlton, A. G., Turpin, B. J.: Particle partitioning potential of organic compounds is highest in the  
837 Eastern US and driven by anthropogenic water, *Atmos. Chem. Phys.*, 13 (20), 10203–10214,  
838 <https://doi.org/10.5194/acp-13-10203-2013>, 2013.

839 Cerully, K. M., Bougiatioti, A., Hite Jr., J. R., Guo, H., Xu, L., Ng, N. L., Weber, R., and Nenes, A.:  
840 On the link between hygroscopicity, volatility, and oxidation state of ambient and water-soluble  
841 aerosol in the Southeastern United States, *Atmos. Chem. Phys.*, 14, 30835–30877,  
842 [https://doi.org/10.5194/acpd-14-30835-](https://doi.org/10.5194/acpd-14-30835-2014) 2014, 2014.

843 Chen, J., Zhao, C. S., Ma, N., Liu, P. F., Göbel, T., Hallbauer, E., Deng, Z. Z., Ran, L., Xu, W. Y.,  
844 Liang, Z., Liu, H. J., Yan, P., Zhou, X. J., and Wiedensohler, A.: A parameterization of low visibilities  
845 for hazy days in the North China Plain, *Atmos. Chem. Phys.*, 12, 4935–4950,  
846 <https://doi.org/10.5194/acp-12-4935-2012>, 2012.

847 Cheng, Y., Zheng, G., Wei, C., Mu, Q., Zheng, B., Wang, Z., Gao, M., Zhang, Q., He, K., Carmichael,  
848 G., Pöschl, U., Su, H.: Reactive nitrogen chemistry in aerosol water as a source of sulfate during

849 haze events in China, *Sci. Adv.*, 2 (12), e1601530, <https://doi.org/10.1126/sciadv.1601530>, 2016.

850 Dougle, P. G., Vlasenko, A. L., Veefkind, J. P., and Brink, H. M. T.: Humidity dependence of the light  
851 scattering by mixtures of ammonium nitrate, ammonium sulfate and soot, *J. Aerosol. Sci.*, 27, 513–  
852 514, [https://doi.org/10.1016/0021-8502\(96\)00329-1](https://doi.org/10.1016/0021-8502(96)00329-1), 1996.

853 Engelhart, G.J., Hildebrandt, L., Kostenidou, E., Mihalopoulos, N., Donahue, N.M., Pandis, S.N.:  
854 Water content of aged aerosol, *Atmos. Chem. Phys.*, 11, 911–920, <https://doi.org/10.5194/acp-11-911-2011>, 2011.

855

856 Ervens, B., Turpin, B. J., Weber, R. J.: Secondary organic aerosol formation in cloud droplets and  
857 aqueous particles (aqSOA): a review of laboratory, field and model studies, *Atmos. Chem. Phys.*,  
858 11 (21), 11069–11102, <https://doi.org/10.5194/acp-11-11069-2011>, 2011.

859 Fountoukis, C. and Nenes, A.: ISORROPIA II: a computationally efficient thermodynamic equilibrium  
860 model for  $K^+$ – $Ca^{2+}$ – $Mg^{2+}$ – $NH_4^+$ – $Na^+$ – $SONO$ – $Cl^-$ – $H_2O$  aerosols, *Atmos. Chem. Phys.*, 7, 4639–  
861 4659, <https://doi.org/10.5194/acp-7-4639-2007>, 2007.

862 Gao, Y., Liu, X., Zhao, C., and Zhang, M.: Emission controls versus meteorological conditions in  
863 determining aerosol concentrations in Beijing during the 2008 Olympic Games, *Atmos. Chem.*  
864 *Phys.*, 11, 12437–12451, <https://doi.org/10.5194/acp-11-12437-2011>, 2011.

865 Gysel, M., Grosier, J., Topping, D.O., Whitehead, J.D., Bower, J.N., Cubison, M.J., Williams, P.I.,  
866 Flynn, M.J., McFiggans, G.B., Coe, H.: Closure study between chemical composition and  
867 hygroscopic growth of aerosol particles during TORCH2, *Atmos. Chem. Phys.*, 7 (24), 6131–6144,  
868 <https://doi.org/10.5194/acp-7-6131-2007>, 2007.

869 Hennigan, C. J., Bergin, M. H., Dibb, J. E., Weber, R. J.: Enhanced secondary organic aerosol  
870 formation due to water uptake by fine particles, *Geophys. Res. Lett.*, 35(18), No. L18801,  
871 <https://doi.org/10.1029/2008GL035046>, 2008.

872 Hodas, N., Sullivan, A. P., Skog, K., Keutsch, F. N., Collett, J. L., Decesari, S., Facchini, M. C.,  
873 Carlton, A. G., Laaksonen, A., Turpin, B. J.: Aerosol Liquid Water Driven by Anthropogenic Nitrate:  
874 Implications for Lifetimes of Water-Soluble Organic Gases and Potential for Secondary Organic  
875 Aerosol Formation, *Environ. Sci. Technol.*, 48 (19), 11127–11136  
876 <https://doi.org/10.1021/es5025096>, 2014.

877 Huang, R., Zhang, Y., Bozzetti, C., Ho, K., Cao, J., Han, Y., Daellenbach, K. R., Slowik, J. G., Platt,  
878 S. M., Canonaco, F.: High secondary aerosol contribution to particulate pollution during haze events  
879 in China, *Nature.*, 514 (7521), 218, <https://doi.org/10.1038/nature13774>, 2014,.

880 Hussein, T., Puustinen, A., Aalto, P. P., Mäkelä, J. M., Hämeri, K., and Kulmala, M.: Urban aerosol  
881 number size distributions, *Atmos. Chem. Phys.*, 4, 391–411, <https://doi.org/10.5194/acp-4-391->

882 2004, 2004.

883 Hussein, T., Dal Maso, M., Petäjä, T., Koponen, I. K., Paatero, P., Aalto, P. P., Hämeri, K., and Kulmala,  
884 M.: Evaluation of an automatic algorithm for fitting the particle number size distributions, *Boreal*  
885 *Environ. Res.*, 10, 337–355, 2005.

886 Jimenez, J. L., Jayne, J. T., Shi, Q., Kolb, C. E., Worsnop, D. R., Yourshaw, I., Morris, J. W.: Ambient  
887 aerosol sampling using the aerodyne aerosol mass spectrometer, *J. Geophys. Res.-Atmos.*, 108(D7),  
888 [https://doi.org/ https://doi.org/10.1029/2001JD001213](https://doi.org/10.1029/2001JD001213), 2003.

889 Kim, Y.P., Seinfeld, J.H., Saxena, P.: Atmospheric gas-aerosol equilibrium I. Thermodynamic model,  
890 *Aerosol Sci. Technol.*, 19 (2), 157–181, <https://doi.org/10.1080/02786829308959628>, 1993.

891 Kitamori, Y., Mochida, M., Kawamura, K.: Assessment of the aerosol water content in urban  
892 atmospheric particles by the hygroscopic growth measurements in Sapporo, Japan. *Atmos. Environ.*,  
893 43 (21), 3416–3423, <https://doi.org/10.1016/j.atmosenv.2009.03.037>, 2009.

894 Kuang Y., Zhao C.S., Ma N., Liu H.J., Bian Y.X., Tao J.C. and Hu M.: Deliquescent phenomena of  
895 ambient aerosols on the North China Plain, *Geophys Res Lett*, 43, 8744-8750,  
896 <https://doi.org/10.1002/2016GL070273>, 2016.

897 Kuang, Y., Zhao, C. S., Zhao, G., Tao, J. C., Xu, W., Ma, N., and Bian, Y. X.: A novel method for  
898 calculating ambient aerosol liquid water content based on measurements of a humidified  
899 nephelometer system, *Atmospheric Measurement Techniques*, 11(5), 2967-2982,  
900 <https://doi.org/10.5194/amt-11-2967-2018>, 2018.

901 Latham, T. L., Beyersdorf, A. J., Thornhill, K. L., Winstead, E. L., Cubison, M. J., Hecobian, A.,  
902 Jimenez, J. L., Weber, R. J., Anderson, B. E., and Nenes, A.: Analysis of CCN activity of Arctic  
903 aerosol and Canadian biomass burning during summer 2008, *Atmos. Chem. Phys.*, 13, 2735–2756,  
904 <https://doi.org/10.5194/acp-13-2735-2013>, 2013.

905 Liao, H., Seinfeld, J. H.: Global impacts of gas-phase chemistry aerosol interactions on direct radiative  
906 forcing by anthropogenic aerosols and ozone, *J. Geophys. Res.-Atmos.*, 110 (D18).  
907 <https://doi.org/10.1029/2005JD005907>, 2005.

908 Li, Z., Lau, W. M., Ramanathan, V., Wu, G., Ding, Y., Manoj, M. G., Liu, J., Qian, Y., Li, J., and Zhou,  
909 T.: Aerosol and mon- soon climate interactions over Asia, *Rev. Geophys.*, 54, 866–929,  
910 <https://doi.org/10.1002/2015RG000500>, 2016.

911 Liu, S., Hu, M., Wu, Z., Wehner, B., Wiedensohler, A., and Cheng, Y.: Aerosol number size distribution  
912 and new particle formation at a rural/coastal site in Pearl River Delta (PRD) of China, *Atmos.*  
913 *Environ.*, 42, 6275–6283, <https://doi.org/10.1016/j.atmosenv.2008.01.063>, 2008.

914 Mei F., Setyan A., Zhang Q. and Wang J.: CCN activity of organic aerosols observed downwind of  
915 urban emissions during CARES, *Atmos. Chem. Phys.*, 13, 12155-12169,

916 <https://doi.org/10.5194/acp-13-12155-2013>, 2013.

917 Moore, R. H., Bahreini, R., Brock, C. A., Froyd, K. D., Cozic, J., Holloway, J. S., Middlebrook, A. M.,  
918 Murphy, D. M., and Nenes, A.: Hygroscopicity and composition of Alaskan Arctic CCN during  
919 April 2008, *Atmos. Chem. Phys.*, 11, 11807–11825, <https://doi.org/10.5194/acp-11-11807-2011>,  
920 2011.

921 Nenes, A., Pandis, S.N., Pilinis, C.: ISORROPIA: a new thermodynamic equilibrium model for  
922 multiphase multicomponent inorganic aerosols, *Aquat. Geochem.*, 4 (1), 123–152,  
923 <https://doi.org/10.1023/A:1009604003981>, 1998.

924 Nguyen, T. K. V., Zhang, Q., Jimenez, J. L., Pike, M., Carlton, A. G.: Liquid Water: Ubiquitous  
925 Contributor to Aerosol Mass, *Environ. Sci. Technol. Lett.*, 3 (7), 257–263,  
926 <https://doi.org/10.1021/acs.estlett.6b00167>, 2016.

927 [Paatero, P., & Tapper, U. \(2010\). Positive matrix factorization: a non-negative factor model with](#)  
928 [optimal utilization of error estimates of data values. \*Environmetrics\*, 5\(2\), 111-126.](#)

929 Petters, M. D. and Kreidenweis, S. M.: A single parameter representation of hygroscopic growth and  
930 cloud condensation nucleus activity, *Atmos. Chem. Phys.*, 7, 1961–1971,  
931 <https://doi.org/10.5194/acp-7-1961-2007>, 2007.

932 Sareen, N., Waxman, E. M., Turpin, B. J., Volkamer, R., Carlton, A. G.: Potential of Aerosol Liquid  
933 Water to Facilitate Organic Aerosol Formation: Assessing Knowledge Gaps about Precursors and  
934 Partitioning, *Environ. Sci. Technol.*, 51 (6), 3327–3335, <https://doi.org/10.1021/acs.est.6b04540>,  
935 2017.

936 Seinfeld, H. J., Pandis, N. S.: *Atmospheric Chemistry and Physics: From Air Pollution to Climate*  
937 *Change*, Taylor & Francis Group, <https://doi.org/10.1080/00139157.1999.10544295>, 2006.

938 Sjogren, S., Gysel, M., Weingartner, E., Baltensperger, U., Cubison, M. J., Coe, H., Zardini, A. A.,  
939 Marcolli, C., Krieger, U. K., and Peter, T.: Hygroscopic growth and water uptake kinetics of two-  
940 phase aerosol particles consisting of ammonium sulfate, adipic and humic acid mixtures, *J. Aerosol*  
941 *Sci.*, 38, 157–171, <https://doi.org/10.1016/j.jaerosci.2006.11.005>, 2007.

942 Song, S., Gao, M., Xu, W., et al.: Possible heterogeneous chemistry of hydroxyl-methane-sulfonate  
943 (HMS) in northern China winter haze, *Atmos. Chem. Phys.*, 19(2): 1357-1371,  
944 <https://doi.org/10.5194/acp-19-1357-2019>, 2019.

945 Stanier, C.O., Khlystov, A.Y., Chan, W.R., Mandiro, M., Pandis, S.N.: A method for the in situ  
946 measurement of fine aerosol water content of ambient aerosols: The Dry Ambient Aerosol Size  
947 Spectrometer (DAASS), *Aerosol Sci. Technol.*, 38 (1), 215–228,  
948 <https://doi.org/10.1080/02786820390229525>, 2004.

949 Stokes, R. H. and Robinson, R. A.: Interactions in aqueous nonelectrolyte solutions. I. Solute-solvent



950 equilibria, *J. Phys. Chem.*, 70, 2126–2131, <https://doi.org/10.1021/j100879a010>, 1966.

951 Sun, Y., Zhuang, G., Tang, A., Wang, Y., An, Z.: Chemical characteristics of PM<sub>2.5</sub> and PM<sub>10</sub> in haze-  
952 fog episodes in Beijing, *Environ. Sci. Technol.*, 40, 3148-3155, <https://doi.org/10.1021/es051533g>,  
953 2006.

954 Sun, Y., Z. F. Wang, P. Q. Fu, T. Yang, Q. Jiang, H. B. Dong, J. Li, and J. J. Jia.: Aerosol composition,  
955 sources and processes during wintertime in Beijing, China, *Atmos. Chem. Phys.*, 13(9), 4577–4592,  
956 <https://doi.org/10.5194/acp-13-4577-2013>, 2013.

957 Sun Y., Chen C., Zhang Y., Xu W., Zhou L., Cheng X., Zheng H., Ji D., Jie L. and Xiao T.: Rapid  
958 formation and evolution of an extreme haze episode in Northern China during winter 2015, *Sci.*  
959 *Rep.*, 6(1):27151, <https://doi.org/10.1038/srep27151>, 2016a.

960 Sun, Y., Wang, Z., Wild, O., Xu, W., Chen, C., Fu, P., Du, W., Zhou, L., Zhang, Q., and Han, T.: “APEC  
961 Blue”: Secondary Aerosol Reductions from Emission Controls in Beijing, *Sci. Rep.*, 6, 20668,  
962 <https://doi.org/10.1038/srep20668>, 2016b.

963 Surratt, J. D., Kroll, J. H., Kleindienst, T. E., Edney, E. O., Claeys, M., Sorooshian, A., Ng, N. L.,  
964 Offenberg, J. H., Lewandowski, M., Jaoui, M., Flagan, R. C., Seinfeld, J. H.: Evidence for  
965 organosulfates in secondary organic aerosol, *Environ. Sci. Technol.*, 41, 517–527,  
966 <https://doi.org/10.1021/es062081q>, 2007.

967 Swietlicki, E., Zhou, J., Berg, O. H., Martinsson, B. G., Frank, G., Cederfelt, S. I., Dusek, U., Berner,  
968 A., Birmili, W., Wiedensohler, A., Yuskiewicz, B., and Bower, K. N.: A closure study of sub-  
969 micrometer aerosol particle hygroscopic behaviour, *Atmos. Res.*, 50, 205–240,  
970 [https://doi.org/10.1016/S0169-8095\(98\)00105-7](https://doi.org/10.1016/S0169-8095(98)00105-7), 1999.

971 Tan, H., Cai, M., Fan, Q., Liu, L., Li, F., & Chan, P. W., et al.: An analysis of aerosol liquid water  
972 content and related impact factors in pearl river delta, *Science of The Total Environment*, 579, 1822-  
973 1830, <https://doi.org/10.1016/j.scitotenv.2016.11.167>, 2017.

974 Tao, W. K., Chen, J. P., Li, Z., Wang, C., and Zhang, C.: Impact of Aerosols on Convective Clouds and  
975 Precipitation, *Rev. Geo. phys.*, 50, 1–62, <https://doi.org/10.1029/2011RG000369>, 2012.

976 Thornton, J. A., Braban, C. F., Abbatt, J. P. D.: N<sub>2</sub>O<sub>5</sub> hydrolysis on sub-micron organic aerosols: the  
977 effect of relative humidity, particle phase, and particle size. *Atmos. Chem. Phys.*, 5 (20), 4593–4603,  
978 <https://doi.org/10.1039/b307498f>, 2003.

979 Topping D O, Mcfiggans G B, Coe H.: A curved multi-component aerosol hygroscopicity model  
980 framework: Part 1 – Inorganic compounds, *Atmos. Chem. Phys.*, 5(5): 1205-1222,  
981 <https://doi.org/10.5194/acp-5-1205-2005>, 2005.

982 Wahner, A., Mentel, T. F., Sohn, M., Stier, J.: Heterogeneous reaction of N<sub>2</sub>O<sub>5</sub> on sodium nitrate

983 aerosol, *J. Geophys. Res. Atmos.*, 103 (D23), 31103–31112, <https://doi.org/10.1029/1998JD100022>,  
984 1998.

985 Wang, G., Zhang, R., Gomez, M. E., Yang, L., Levy Zamora, M., Hu, M., Lin, Y., Peng, J., Guo, S.,  
986 Meng, J., Li, J., Cheng, C., Hu, T., Ren, Y., Wang, Y., Gao, J., Cao, J., An, Z., Zhou, W., Li, G.,  
987 Wang, J., Tian, P., MarreroOrtiz, W., Secrest, J., Du, Z., Zheng, J., Shang, D., Zeng, L., Shao, M.,  
988 Wang, W., Huang, Y., Wang, Y., Zhu, Y., Li, Y., Hu, J., Pan, B., Cai, L., Cheng, Y., Ji, Y., Zhang, F.,  
989 Rosenfeld, D., Liss, P. S., Duce, R. A., Kolb, C. E., Molina, M. J.: Persistent sulfate formation from  
990 London Fog to Chinese haze, *Proc. Natl. Acad. Sci. U. S. A.*, 113 (48), 13630–13635,  
991 <https://doi.org/10.1073/pnas.1616540113>, 2016.

992 Wang, H., Lu, K., Chen, X., Zhu, Q., Chen, Q., Guo, S., Jiang, M., Li, X., Shang, D., Tan, Z., Wu, Y.,  
993 Wu, Z., Zou, Q., Zheng, Y., Zeng, L., Zhu, T., Hu, M., Zhang, Y.: High N<sub>2</sub>O<sub>5</sub> Concentrations  
994 Observed in Urban Beijing: Implications of a Large Nitrate Formation Pathway, *Environ. Sci.*  
995 *Technol. Lett.*, 4 (10), 416–420, <https://doi.org/10.1021/acs.estlett.7b00341>, 2017.

996 Wang, T., Nie, W., Gao, J., Xue, L. K., Gao, X. M., Wang, X. F., Qiu, J., Poon, C. N., Meinardi, S.,  
997 Blake, D., Wang, S. L., Ding, A. J., Chai, F. H., Zhang, Q. Z., and Wang, W. X.: Air quality during  
998 the 2008 Beijing Olympics: secondary pollutants and regional impact, *Atmos. Chem. Phys.*, 10,  
999 7603–7615, <https://doi.org/10.5194/acp-10-7603-2010>, 2010.

1000 Wang, Y., Zhang, Q., Jiang, J., Zhou, W., Wang, B., He, K., Duan, F., Zhang, Q., Philip, S., and Xie,  
1001 Y.: Enhanced sulfate formation during China’s severe winter haze episode in January 2013 missing  
1002 from current models, *J. Geophys. Res.-Atmos.*, 119, 10425– 10440,  
1003 <https://doi.org/10.1002/2013JD021426>, 2014.

1004 Wang Y., Zhang F., Li Z., Tan H., Xu H., Ren J., Zhao J., Du W. and Sun Y.: Enhanced hydrophobicity  
1005 and volatility of submicron aerosols under severe emission control conditions in Beijing, *Atmos*  
1006 *Chem Phys*, 17, 5239-5251, <https://doi.org/10.5194/acp-17-5239-2017>, 2017.

1007 Wang Y., Li Z., Zhang Y., Du W., Zhang F., Tan H., Xu H., Fan T., Jin X., Fan X., Dong Z., Wang Q.  
1008 and Sun Y.: Characterization of aerosol hygroscopicity, mixing state, and CCN activity at a suburban  
1009 site in the central North China Plain, *Atmos. Chem. Phys.*, 18, 11739-11752,  
1010 <https://doi.org/10.5194/acp-18-11739-2018>, 2018.

1011 Wehner, B., Birmili, W., Ditas, F., Wu, Z., Hu, M., Liu, X., Mao, J., Sugimoto, N., and Wiedensohler,  
1012 A.: Relationships between sub micrometer particulate air pollution and air mass history in Beijing,  
1013 China, 2004–2006, *Atmos. Chem. Phys.*, 8, 6155–6168, <https://doi.org/10.5194/acp-8-6155-2008>,  
1014 2008.

1015 Wexler, A.S., Clegg, S.L.: Atmospheric aerosol models for systems including the ions H<sup>+</sup>, NH<sub>4</sub><sup>+</sup>, Na<sup>+</sup>,  
1016 SO<sub>4</sub><sup>2-</sup>, NO<sub>3</sub><sup>-</sup>, Cl<sup>-</sup>, Br<sup>-</sup>, and H<sub>2</sub>O, *J. Geophys. Res.-Atmos.*, 107 (D14): 14-14,

1017 <https://doi.org/10.1029/2001JD000451>, 2002.

1018 Whitby, K. T.: The physical characteristics of sulfur aerosols, *Atmos. Environ.*, 12, 135–159,  
1019 <https://doi.org/10.1016/j.atmosenv.2007.10.057>, 1978.

1020 Wiedensohler A.: An approximation of the bipolar charge distribution for particles in the submicron  
1021 size range, *J. Aerosol Sci.*, 19, 387–389, [https://doi.org/10.1016/0021-8502\(88\)90278-9](https://doi.org/10.1016/0021-8502(88)90278-9), 1988.

1022 Wu, G. X., Li, Z. Q., Fu, C. B., Zhang, X. Y., Zhang, R. Y., Zhang, R. H., Zhou, T. J., Li, J. P., Li, J.  
1023 D., and Zhou, D. G.: Advances in studying interactions between aerosols and monsoon in China,  
1024 *Science China Earth Science*, 59, 1–16, <https://doi.org/10.1007/s11430-015-5198-z>, 2016.

1025 Wu, Z., Wang, Y., Tan, T., Zhu, Y., Li, M., & Shang, D., et al.: Aerosol liquid water driven by  
1026 anthropogenic inorganic salts: implying its key role in the haze formation over north china  
1027 plain, *Environ. Sci. Technol. Lett.*, 5(3), 160-166, <https://doi.org/10.1021/acs.estlett.8b00021>, 2018.

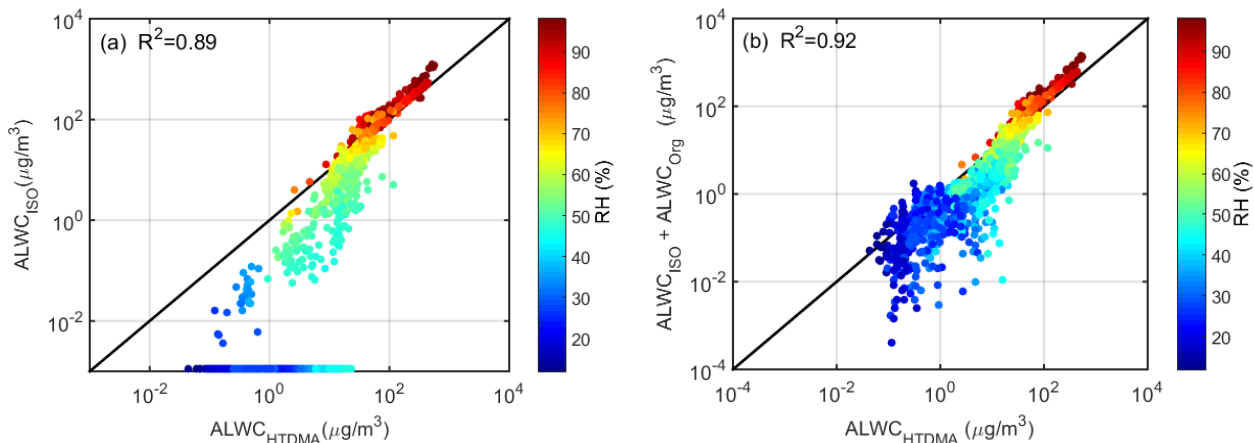
1028 Xu, L., Guo, H., Boyd, C. M., Klein, M., Bougiatioti, A., Cerully, K. M., Hite, J. R., Isaacman-  
1029 VanWertz, G., Kreisberg, N. M., Knote, C., Olson, K., Koss, A., Goldstein, A. H., Hering, S. V., de  
1030 Gouw, J., Baumann, K., Lee, S.-H., Nenes, A., Weber, R. J., and Ng, N. L.: Effects of anthropogenic  
1031 emissions on aerosol formation from isoprene and monoterpenes in the southeastern United States,  
1032 *P. Natl. Acad. Sci.*, 112, 37–42, <https://doi.org/10.1073/pnas.1417609112>, 2015.

1033 Xu, W., Han, T., Du, W., Wang, Q., Chen, C., Zhao, J., Zhang, Y., Li, J., Fu, P., Wang, Z., Worsnop, D.  
1034 R., Sun, Y.: Effects of Aqueous- Phase and Photochemical Processing on Secondary Organic  
1035 Aerosol Formation and Evolution in Beijing, China, *Environ. Sci. Technol. Lett.*, 51 (2), 762–770,  
1036 <https://doi.org/10.1021/acs.est.6b04498>, 2017.

1037 Zheng, B., Zhang, Q., Zhang, Y., He, K. B., Wang, K., Zheng, G. J., Duan, F. K., Ma, Y. L., Kimoto,  
1038 T.: Heterogeneous chemistry: a mechanism missing in current models to explain secondary  
1039 inorganic aerosol formation during the January 2013 haze episode in North China, *Atmos. Chem.  
1040 Phys.*, 15 (4), 2031–2049, <https://doi.org/10.5194/acp-15-2031-2015>, 2015.

1041 Zieger, P., Väisänen, O., Corbin, J. C., Partridge, D. G., Bastelberger, S., Mousavi-Fard, M., Rosati,  
1042 B., Gysel, M., Krieger, U. K., Leck, C., Nenes, A., Riipinen, I., Virtanen, A., and Salter, M. E.:  
1043 Revising the hygroscopicity of inorganic sea salt particles, *Nature communications*, 8, 15883,  
1044 <https://doi.org/10.1038/ncomms15883>, 2017.

1045  
1046



1047

1048

**Figure 1. Comparison between  $ALWC_{HTDMA}$  and (a)  $ALWC_{ISO}$  and (b) the sum of  $ALWC_{ISO}$  and  $ALWC_{Org}$ .**

1049

$ALWC_{HTDMA}$  refers to calculated ALWC based on the measured growth factor and PNSDs,  $ALWC_{ISO}$  refers to

1050

simulated ALWC from the ISORROPIA II model, and  $ALWC_{Org}$  refers to the inferred ALWC contributed by

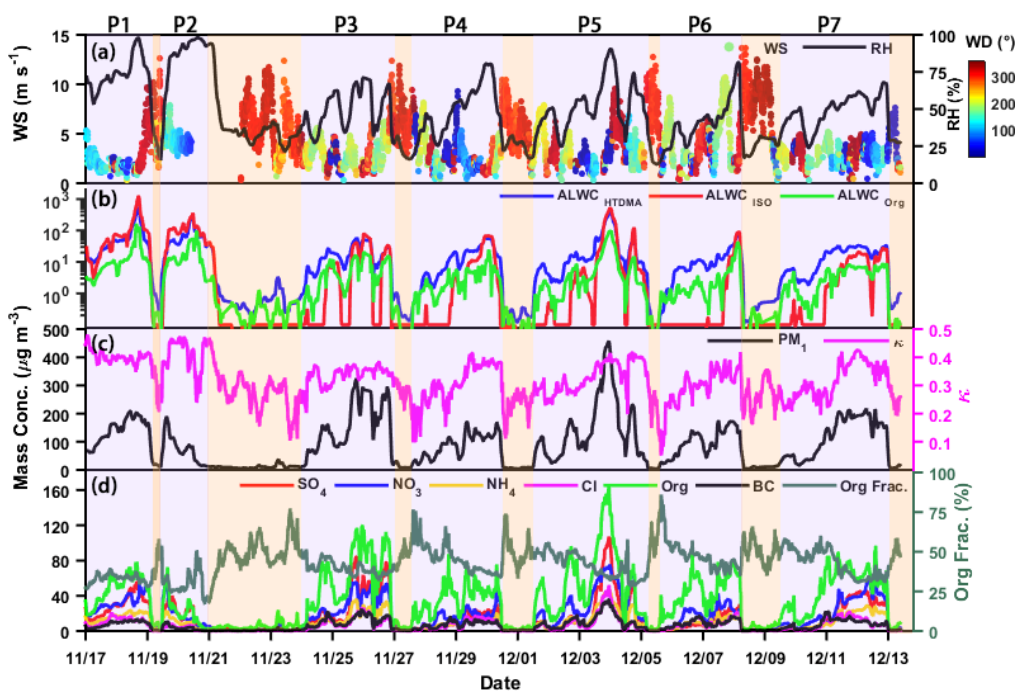
1051

organic species. The coefficient of determination  $R^2$  is given in each panel. The color of the dots denotes the ambient

1052

RH; the solid line denotes the 1:1 line.

1053



1054

**Figure 2. Time series of (a) wind speed (WS, left y-axis), ambient relative humidity (RH, right y-axis), and wind**

1056

**direction (WD, colored dots), (b)  $ALWC_{HTDMA}$  (in blue),  $ALWC_{ISO}$  (in red), and  $ALWC_{Org}$  (in green), (c)  $PM_1$  mass**

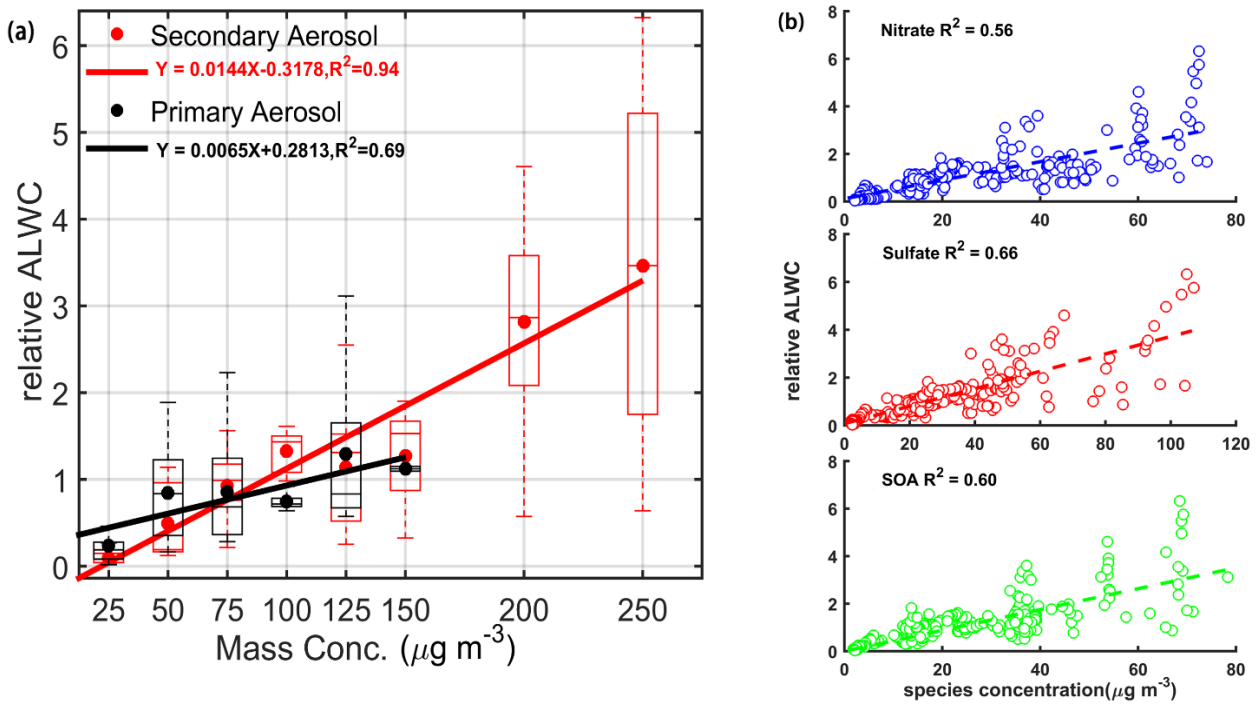
1057

**concentration (left y-axis) and hygroscopicity parameter ( $\kappa$ , right y-axis) calculated using the ZSR model described**

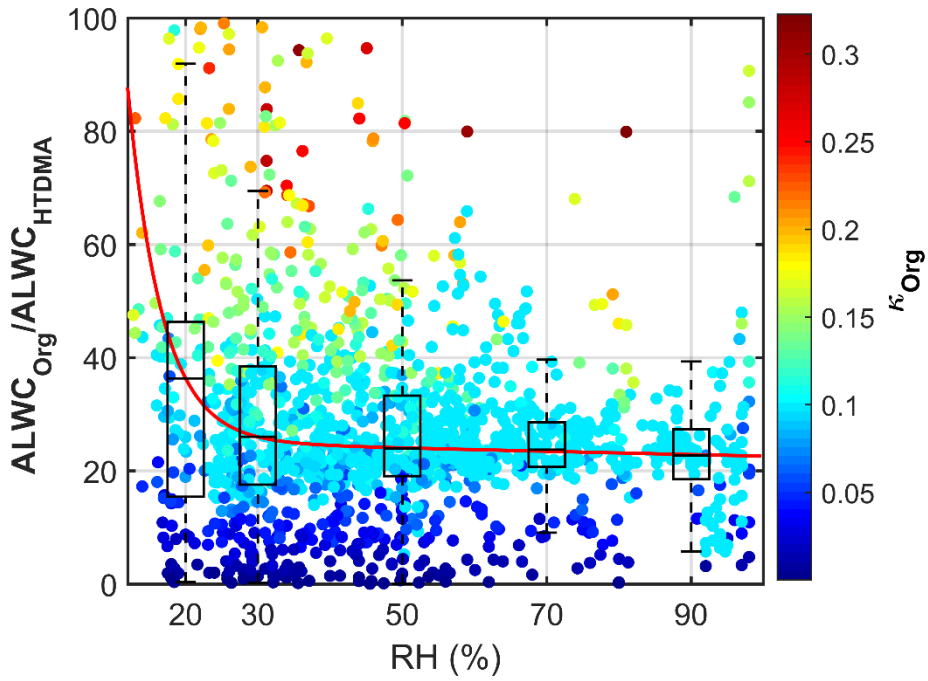
1058

**by Eq. (7), and (d) mass concentrations of aerosol species in  $PM_1$  (left y-axis) and organic aerosol mass fraction**

1059 (right y-axis). Seven polluted episodes (segments of the time series with a purple background) are selected for  
 1060 examination.  
 1061



1062  
 1063 **Figure 3.** The correlation analysis between relative ALWC and (a) primary (in black) and secondary (in red) aerosol  
 1064 mass concentrations, and (b) nitrate, sulfate, and secondary organic aerosol (SOA) mass concentrations. Panel (a)  
 1065 shows mean relative ALWCs (solid dots) with boxes showing the 25th, 50th, and 75th percentiles. The extremities  
 1066 show the 5th and 95th percentiles. The solid lines in (a) and the dashed lines in (b) both represent the corresponding  
 1067 best-fit lines from linear regression.



1068

1069

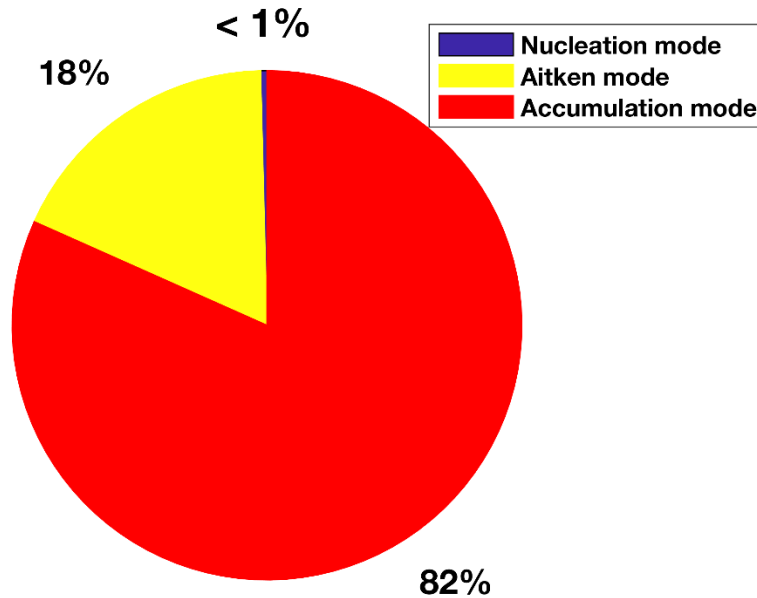
1070

1071

1072

1073

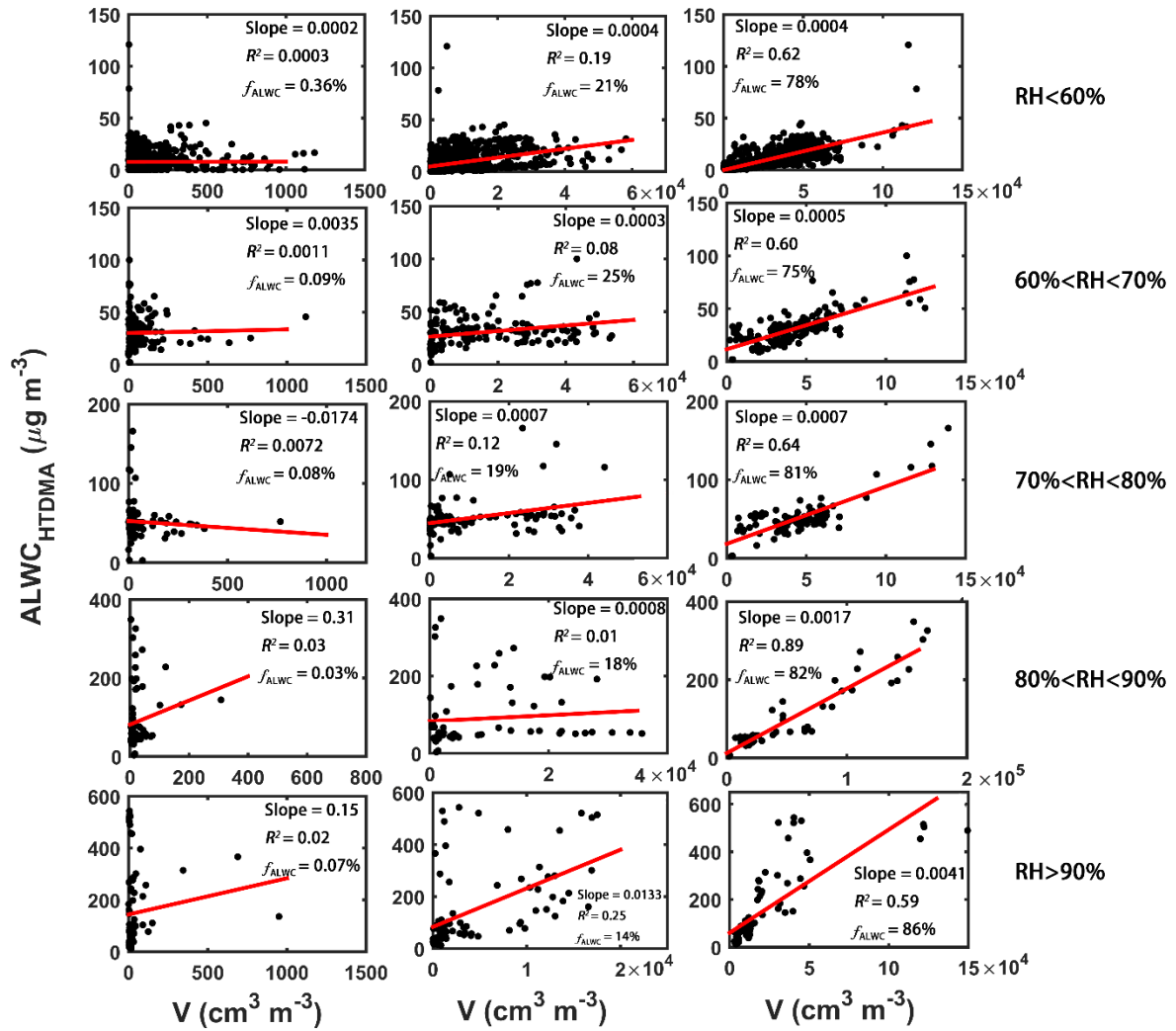
**Figure 4.** The variation of the fraction of  $ALWC_{Org}$  in total  $ALWC$  ( $ALWC_{HTDMA}$ ) with the ambient relative humidity (RH). The color of the dots denotes the hygroscopicity parameter of organics ( $\kappa_{Org}$ ). The boxes show the fraction of  $ALWC_{Org}$  with the 25th, 50th, and 75th percentiles. The extremities show the 5th and 95th percentiles. The red line shows the fitting curve with the function  $y = ae^{bx}$ .



1074

1075

**Figure 5.** The contribution of particles different modes to  $ALWC_{HTDMA}$



1076

1077

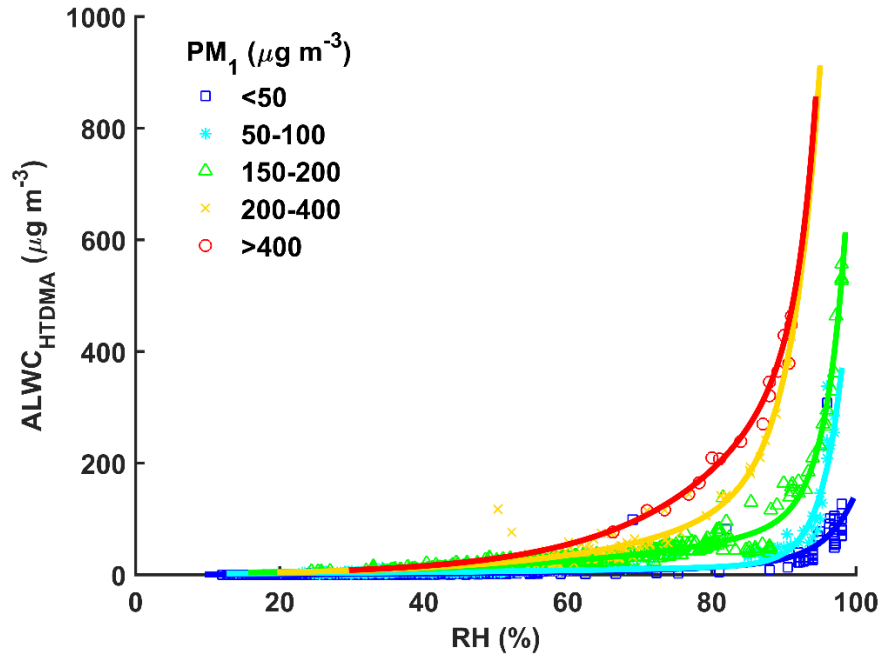
1078

1079

1080

1081

Figure 64. The correlation analysis between  $ALWC_{HTDMA}$  and the volume concentration of nucleation mode (left column), Aitken mode (middle column), and accumulation mode (right column) particles under different ambient relative humidity (RH) conditions. The average contribution of each mode particles to ALWC under different ambient RH conditions is denoted by  $f_{ALWC}$ . The red lines represent the best-fit lines from linear regression.



1082

1083

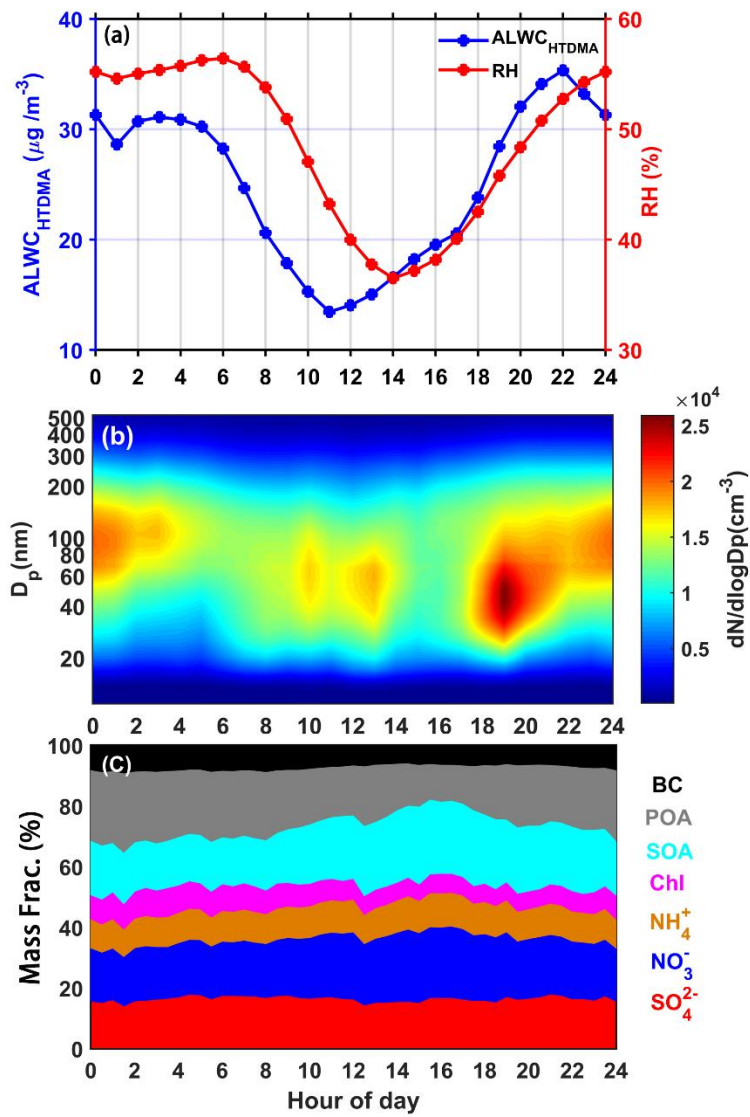
1084

1085

1086

Figure 75. The dots show how  $ALWC_{HTDMA}$  varies with the ambient relative humidity (RH) for different  $PM_1$  mass concentration ranges (colored symbols). The colored curves represent the best-fit lines through the data using the fitting function-  $y = ae^{bx}$ .





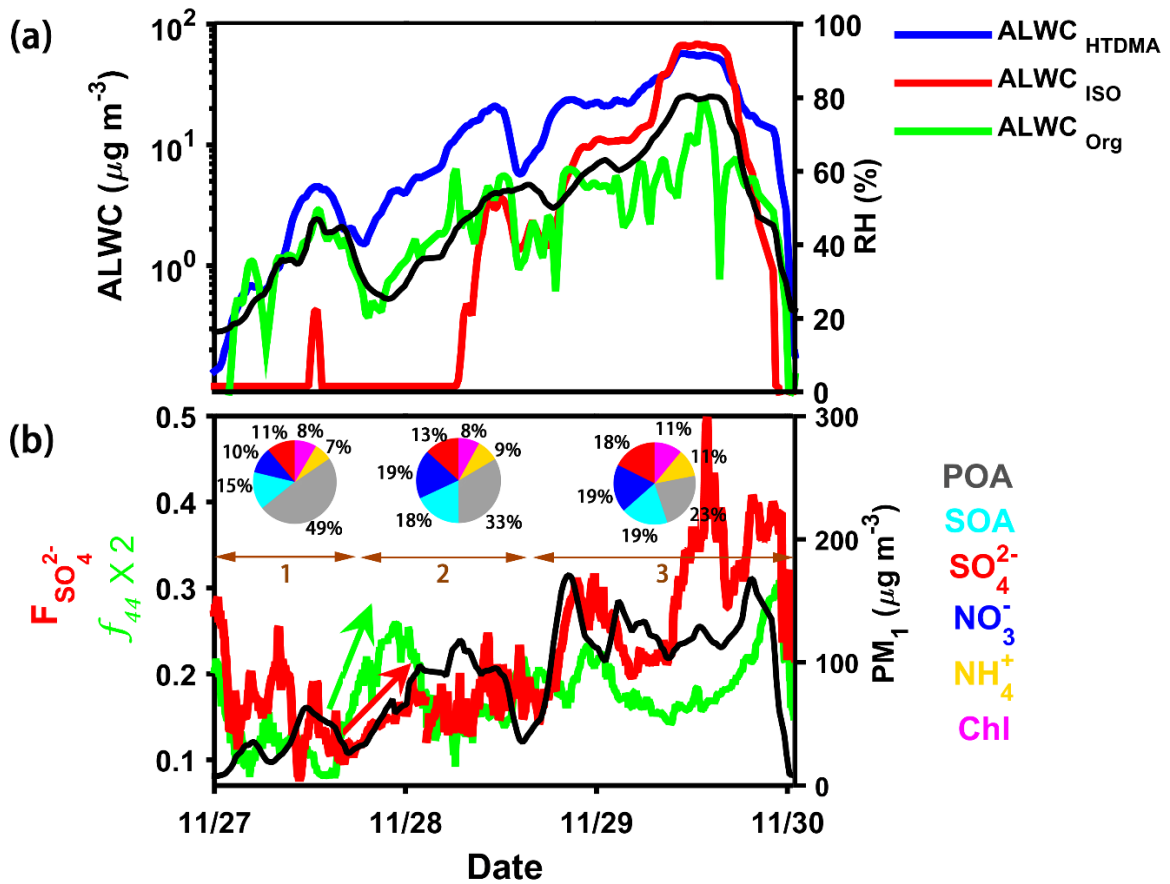
1087

1088

1089

1090

Figure 86. Diurnal variations of (a) ALWC<sub>HTDMA</sub> (in blue) and ambient RH (in red), (b) particle number size distribution, and (c) the mass fraction of different chemical species. The time is in Beijing time.



1091

1092

1093

1094

1095

1096

1097

Figure 97. Time series of (a)  $ALWC_{HTDMA}$  (in blue),  $ALWC_{ISO}$  (in red),  $ALWC_{Org}$  (in green), and RH (right y-axis), and (b) the sulfur oxidation ratio ( $F_{SO_4^{2-}}$ ),  $f_{44}$ , and  $PM_{10}$  mass concentration (right y-axis) during the P4 case in Figure 2. The pie charts in (b) represent the average chemical compositions of  $PM_{10}$  during three stages of the pollution event (denoted by brown horizontal lines). The red and green arrows in (b) indicate the rapid increase in  $F_{SO_4^{2-}}$  and  $f_{44}$  at the initial stage.